Ninth and Tenth Order Virial Coefficients for Hard Spheres in *D* Dimensions

Nathan Clisby[1] and Barry M. McCoy[2]

We evaluate the virial coefficients B_k for $k \leq 10$ for hard spheres in dimensions $D = 2, \cdots, 8$. Virial coefficients with k even are found to be negative when $D \geq 5$. This provides strong evidence that the leading singularity for the virial series lies away from the positive real axis when $D \geq 5$. Further analysis provides evidence that negative virial coefficients will be seen for some $k > 10$ for $D = 4$, and there is a distinct possibility that negative virial coefficients will also eventually occur for $D = 3$.

KEY WORDS: Hard spheres; virial expansion.

1. INTRODUCTION

The hard sphere gas of particles of diameter σ in D dimensions defined by the two body potential

$$U(\mathbf{r}) = \begin{cases} +\infty & |\mathbf{r}| < \sigma \\ 0 & |\mathbf{r}| > \sigma \end{cases} \tag{1}$$

is one of the oldest and most studied systems in statistical mechanics. Nevertheless after more than a century after the initial work of van der Waals[1], Boltzmann[2], and van Laar[3] who computed the coefficients up through B_4 in three dimensions for the low density virial expansion of the pressure

$$\frac{P}{k_B T} = \sum_{k=1}^{\infty} B_k \rho^k \quad \text{with } B_1 \equiv 1 \tag{2}$$

[1] ARC Centre of Excellence for Mathematics and Statistics of Complex Systems, 139 Barry Street, The University of Melbourne, Parkville Victoria 3010 Australia; e-mail: N.clisby@ms.unimelb.edu.au
[2] C. N. Yang Institute for Theoretical Physics, Stony Brook University, Stony Brook, NY 11794-3840, U.S.A.; e-mail: mccoy@insti.physics.sunysb.edu

there are still basic features of this system which are unresolved and controversial. Chief among these properties are 1) the radius of convergence of the virial series, 2) the question of the occurrence of negative virial coefficients in 2 and 3 dimensions, and 3) the analytic demonstration of the freezing phase transition which was first seen in computer experiments[4,5] in the late 1950s.

The analytic information available for the hard sphere gas is extremely sparse. Indeed, outside of B_2 and B_3 which are elementary to compute and the original computation of B_4 in $D = 3$ by Boltzmann and van Laar, the only other analytic computations of virial coefficients are of B_4 in $D = 2$ done simultaneously by Rowlinson[6] and Hemmer[7] in 1964, and the recent computation by the present authors[8] of B_4 for $D = 4, 6, 8, 10, 12$, and by Lyberg[9] for odd dimensions $D = 5, 7, 9, 11$.

All other computations for the hard sphere gas are by means of computer. The fifth virial coefficient was first calculated numerically in the 1950s for hard discs by Metropolis et al.[10] and for hard spheres by Rosenbluth and Rosenbluth[11]. An extensive and systematic effort to numerically calculate the virial coefficients B_5, B_6, and B_7 for two and three dimensions was carried out by Ree and Hoover [12,13,14] during the 1960s. The coefficient B_8 in $D = 2$ and 3 was computed by Janse van Rensburg[15] in 1993. Vlasov, You, and Masters[16] recently recalculated B_7 and B_8, and Labík, Kolafa, and Malijevský[17,18] have recalculated the virial coefficients to B_8 and also calculated B_9. All these virial coefficients are positive.

The study of virial coefficients for dimensions greater than 3 was initiated in 1964 by Ree and Hoover[19] who computed B_4 for $D = 4, \cdots, 11$ and found for $D \geq 8$ that B_4 is negative. This was the first time that any negative virial coefficient had been seen for the hard sphere system. The coefficients B_5 and B_6 for $D = 4$ and 5 were computed by Bishop, Masters, and Clarke[20] in 1999, and Bishop, Masters, and Vlasov[21,22] have recently calculated B_7 in dimensions four and five, and B_8 in four and five dimensions. Other recent studies of hard hyperspheres include[23,24], and Frisch et al.[25] and later Frisch and Percus[26] have studied the virial expansion in high dimensions, and in particular in the limit as the dimension approaches infinity. The present authors recently extended[27] the study of B_4, B_5, and B_6 up to dimension $D = 50$. In this study it was found that B_5 is always positive but the B_6 is negative for $D \geq 6$.

There are two very important observations to be made about these computations.

The first observation is that the virial coefficients B_2 through B_8 in $D = 2, 3$ have been analyzed by many authors in an attempt to find an approximate equation of state. These approximations are reviewed in Subsection 4.3. Without exception all of these studies have the remarkable feature that they show no singularity at the density at which the computer studies indicates that the system freezes. Indeed some of the approximate equations of state are analytic for real positive densities greater than the density of closest packed discs and spheres. One interpretation

of this is that the first eight virial coefficients are not sufficient to see the true asymptotic behavior of B_k for large k.

The second observation is that because B_4 changes sign between $D = 7$ and $D = 8$, and B_6 changes sign between $D = 5$ and 6 it may be for large k that B_k can become negative for dimensions smaller than 5. In particular if for $D = 2$ or $D = 3$ there were a value of k such that B_k changed sign then the approximate equations of state obtained from the first eight virial coefficients would be wholly inadequate to obtain the radius of convergence of the virial series.

In this paper we address the questions of the radius of convergence and the negativity of the virial coefficients by numerically computing B_7 for $D = 6, 7, 8$, B_8 for $D = 5, \cdots, 8$, and B_9 and B_{10} for $D = 2, \cdots, 8$. Our results are given in Table 1. For the Monte Carlo integration we use the formulation of Ree and Hoover[12,13]. For hard spheres it is well known that in any dimension D there may be some Ree-Hoover diagrams which vanish identically for geometric reasons. The determination of the number of such geometrically excluded diagrams is an interesting problem in its own right and our results for this are given in Table 2.

In Section 2 we discuss the virial expansion and the theoretical framework for the problem of calculating virial coefficients for hard spheres. In Section 3 we explain our method of computation with particular emphasis on what needs to be done to handle the 4,980,756 Ree-Hoover diagrams contributing to B_{10} in an efficient fashion. In Section 4 we provide information about the hard sphere system relevant to the understanding of the asymptotic behavior of the virial series. In Section 5 we address the question of the large k behavior of B_k. We propose in Subsection 5.1 two complementary criteria which B_k should satisfy in order to be considered asymptotic. We discuss the asymptotic behavior of the virial series in 5.2 from a ratio analysis. In Subsection 5.3 we apply the methods of Padé approximants and differential approximants to the ten known coefficients. We conclude in Section 6 with a summary of key results.

The results of this work as well as the papers of Clisby and McCoy[8,27] are included in the dissertation of Clisby[28].

2. VIRIAL EXPANSION

To calculate virial coefficients we use the reformulation of the Mayer series[30] carried out by Ree and Hoover[13].

In the Mayer formulation virial coefficients B_k are given as the sum of integrals which may be represented by biconnected graphs of k points. We define a k point graph G as a set of vertices $V = \{v_i, i = 1, \cdots, k\}$ together with a set of edges E whose elements are pairs (u, v) where $u, v \epsilon V$. We will only be interested in undirected graphs, and not in generalizations such as directed graphs or graphs with multiple edges and loops. A graph is biconnected if there are no vertices whose removal would result in a disconnected graph, which are more concisely

Table I. Numerical values of virial coefficients. Values for B_7 $D > 5$, B_8 $D > 4$, B_9, and B_{10} are new, and other values improve on published literature results for B_5 and higher except for the results for B_5 for $D = 2, 3$ which are due to Kratky[29]

D	B_3/B_2^2	B_4/B_2^3	B_5/B_2^4	B_6/B_2^5	B_7/B_2^6	B_8/B_2^7	B_9/B_2^8	B_{10}/B_2^9
2	0.782004···	0.53223180···	0.33355604(1)*	0.1988425(42)	0.1148728(43)	0.0649930(34)	0.0362193(35)	0.0199537(80)
3	0.625	0.2869495···	0.1102252(1)*	0.03888198(91)	0.01302354(91)	0.0041832(11)	0.0013094(13)	0.0004035(15)
4	0.5063340···	0.15184606···	0.0357041(17)	0.0077359(16)	0.0014303(19)	0.0002888(18)	0.0000441(22)	0.0000113(31)
5	0.414063···	0.0759724807···	0.01295551(13)	0.0009815(14)	0.0004162(19)	−0.0001120(20)	0.0000747(26)	−0.00000492(48)
6	0.340941···	0.03336314···	0.0075231(11)	−0.0017385(13)	0.0013066(18)	−0.0008950(30)	0.0006673(45)	−0.000525(16)
7	0.282227···	0.009864994662···	0.0070724(10)	−0.0035121(11)	0.0025386(16)	−0.0019937(28)	0.0016869(41)	−0.001514(14)
8	0.234614···	−0.00255768···	0.00743092(93)	−0.0045164(11)	0.0034149(15)	−0.0028624(26)	0.0025969(38)	−0.002511(13)

Table II. Number of Mayer and Ree-Hoover integrals

					Order				
	2	3	4	5	6	7	8	9	10
Mayer	1	1	3	10	56	468	7123	194066	9743542
RH	1	1	2	5	23	171	2606	81564	4980756
RH/Mayer	1	1	0.667	0.500	0.410	0.365	0.366	0.420	0.511
RH, $D = 1$	1	1	1	1	1	1	1	1	1
RH, $D = 2$	1	1	2	4	15	73	$\gtrsim 647$	$\gtrsim 8417$	$\gtrsim 110529$
RH, $D = 3$	1	1	2	5	22	161	>2334	>60902	
RH, $D = 4$	1	1	2	5	23	169	>2556	>76318	

known as articulation points. Then the virial coefficient at order k is given in the Mayer formalism by

$$B_k = \frac{1-k}{k!} \sum_{G \in \mathscr{B}_k^L} S(G)$$

$$= \frac{1-k}{k!} \sum_{G \in \mathscr{B}_k^U} C(G)S(G) \tag{3}$$

where $S(G)$ is the value of the integral represented by G, $\mathscr{B}_k^L$ is the set of all labeled, biconnected graphs, $\mathscr{B}_k^U$ is the set of all unlabeled biconnected graphs. $C(G)$ is a combinatorial factor which is defined as the total number of distinguishable labelings of a graph, otherwise given as:

$$C(G) = \frac{k!}{|\text{Aut}(G)|} \tag{4}$$

for a graph with k vertices, and $|\text{Aut}(G)|$ is the cardinality of the automorphism group of the graph.

Each graph may be identified with an integral in which the vertices represent coordinates in D–dimensional Euclidean space, and a bond between vertices i and j represents the function

$$f(\mathbf{r_i} - \mathbf{r_j}) = \exp(-U(\mathbf{r_i} - \mathbf{r_j})/k_B T) - 1 \tag{5}$$

For example, the integral corresponding to the graph in Fig. 1 may be written as

$$S(G_{\text{ex}}) = \lim_{V \to \infty} \frac{1}{V} \int d^D \mathbf{r_1} d^D \mathbf{r_2} d^D \mathbf{r_3} d^D \mathbf{r_4} \, f(\mathbf{r_{12}}) f(\mathbf{r_{23}}) f(\mathbf{r_{14}}) f(\mathbf{r_{34}})$$

$$= \int d^D \mathbf{r_1} d^D \mathbf{r_2} d^D \mathbf{r_3} \, f(\mathbf{r_{12}}) f(\mathbf{r_{23}}) f(\mathbf{r_1}) f(\mathbf{r_3}) \tag{6}$$
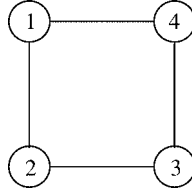
Fig. 1. Typical labeled graph, G_{ex}.

where $\mathbf{r_{ij}} = \mathbf{r_i} - \mathbf{r_j}$, and V is the volume to be integrated over. In the second expression for the integral, $\mathbf{r_4}$ is defined as the origin. Naturally the value of the integral does not depend on the labeling chosen, and this is the reason that in Eq. 3 the sum over labeled graphs can be converted to a sum over unlabeled graphs.

A useful re-summation was performed by Ree and Hoover[12,13] by introducing the function

$$\tilde{f}(\mathbf{r}) = 1 + f(\mathbf{r}) = \exp(-U(\mathbf{r})/k_B T) \tag{7}$$

and then expanding each Mayer graph by substituting $1 = \tilde{f} - f$ for pairs of vertices not connected by f bonds. This method was previously used by Percus and Yevick[31] in comparing the exact values of the fourth and fifth virial coefficients with coefficients obtained from the Percus–Yevick equation, and by Percus[32] in discussing the derivation of the Percus–Yevick equation. One can see that upon performing this re-summation on the Mayer series that vertices in the resultant graphs will all be mutually connected by either f bonds or $\tilde{f}$ bonds, and that graphs must be biconnected with respect to f bonds. In this paper, we adopt the convention that graph edges only correspond to f bonds; in other contexts it can be very useful to refer to the complement graphs in which the $\tilde{f}$ bonds are edges. Now there is an additional factor for each labeled graph, called the star content by Ree and Hoover, which may be either positive or negative, and is equal to the total number of biconnected subgraphs with an even number of edges removed (including zero), subtract the number of biconnected subgraphs with an odd number of edges removed. Thus the Ree-Hoover expression for the virial coefficient B_k is

$$B_k = \frac{1-k}{k!} \sum_{G \epsilon \mathcal{B}_k^L} \mathrm{SC}(G)\tilde{S}(G)$$

$$= \frac{1-k}{k!} \sum_{G \epsilon \mathcal{B}_k^U} C(G)\mathrm{SC}(G)\tilde{S}(G) \tag{8}$$

where $\mathrm{SC}(G)$ is the star content and $\tilde{S}(G)$ is the Ree-Hoover integral value of the graph G. As a consequence of the fact that for every 1 expanded there is a positive

and negative coefficient, in the Ree-Hoover re-summation only the complete graph which has no 1's contributes a net non-zero amount. Thus

$$\sum_{G \in \mathcal{B}_k^L} SC(G) = 1 \tag{9}$$

Now, to compare with the Mayer integral formalism of Eq. 6 we give the expression for the Ree-Hoover integral represented by Fig. 2

$$\tilde{S}(G_{\text{ex}}) = \lim_{V \to \infty} \frac{1}{V} \int d^D\mathbf{r_1} d^D\mathbf{r_2} d^D\mathbf{r_3} d^D\mathbf{r_4} f(\mathbf{r_{12}}) \tilde{f}(\mathbf{r_{13}}) f(\mathbf{r_{23}}) f(\mathbf{r_{14}}) \tilde{f}(\mathbf{r_{24}}) f(\mathbf{r_{34}})$$

$$= \int d^D\mathbf{r_1} d^D\mathbf{r_2} d^D\mathbf{r_3} f(\mathbf{r_{12}}) \tilde{f}(\mathbf{r_{13}}) f(\mathbf{r_{23}}) f(\mathbf{r_1}) \tilde{f}(\mathbf{r_2}) f(\mathbf{r_3}) \tag{10}$$

In the case of hard spheres, the potential is given by Eq. 1, and so $f(\mathbf{r})$ and $\tilde{f}(\mathbf{r})$ are particularly simple:

$$f(\mathbf{r}) = \begin{cases} -1 & |\mathbf{r}| < \sigma \\ 0 & |\mathbf{r}| > \sigma \end{cases} \tag{11}$$

$$\tilde{f}(\mathbf{r}) = \begin{cases} 0 & |\mathbf{r}| < \sigma \\ +1 & |\mathbf{r}| > \sigma \end{cases} \tag{12}$$

The f bonds force vertices to be close together, while $\tilde{f}$ bonds force vertices apart. These competing conditions may mean that for some graphs contributing to B_k in dimension $D < k - 1$ there are no point configurations that satisfy the conditions, and hence the corresponding integral would be zero for geometric reasons. Any configuration of points in D–dimensional Euclidean space can contribute to at most one Ree-Hoover diagram, whereas it may contribute to many Mayer diagrams, and in particular for all k point graphs G

$$|S(G)| \geq |\tilde{S}(G)| \tag{13}$$

The inequality is strict when one excludes the complete star graph. This leads to the primary advantage of the Ree-Hoover formulation over the original Mayer formulation: it greatly reduces the degree of cancellation between positive and negative diagrams.

3. METHOD

In Section 3.1 we give a broad description for the Monte Carlo algorithm used to perform the numerical integration for our results of Table 1. In Section 3.2 we define some graph theory notation that is necessary for our detailed discussion of the calculation of the star content of all unlabeled graphs of up to ten points in Section 3.3, the determination of a minimal set of spanning trees to generate configurations for the Monte Carlo algorithm in Section 3.4, and the unlabeling

factor for graphs of up to ten points in Section 3.5. Lastly, in Section 3.6 we give specific details of the implementation of the algorithm.

3.1. Monte Carlo Algorithm

We calculate virial coefficients via the hit or miss Monte Carlo integration algorithm described by Ree and Hoover[12]. Monte Carlo integration is appropriate for high dimensional integrals, which is certainly the case for the integrals we calculate as in general, the calculation of B_k for D dimensions is a $(k-1)D$ dimensional integral.

If we need to integrate a function $F(x)$ over a complicated, high dimensional domain D_1, the hit or miss Monte Carlo method works by enlarging the domain of integration to a simple, easily characterized domain D_2 and setting the function to zero in $D_2 \setminus D_1$. We then select points uniformly from within D_2 using a pseudo random number generator, and the integral we are interested in is given as the volume of the enlarged domain $V(D_2)$ multiplied by the mean value of $F(x)$ over D_2.

$$\int_{D_1} dx \ F(x) = \int_{D_2} dx \ F(x) \quad D_1 \subset D_2, \ F(x) \equiv 0 \ \forall x \in D_2 \setminus D_1$$

$$= V(D_2) \lim_{N \to \infty} \frac{1}{N} \sum_{i=1}^{N} F(x_i) \qquad x_i \in D_2 \tag{14}$$

The Ree-Hoover integral of a given k point biconnected graph G has a trivial integrand which is ± 1, but the domain is all configurations $(r_1, r_2, \cdots, r_k)$ where $r_i \in \mathbf{R}^D$ and the resulting point set may be identified with G. To calculate the integral, we first identify a spanning tree of the graph, and use all Ree-Hoover diagrams which are spanned by this tree as the enlarged domain. To generate random configurations in the Monte Carlo algorithm we place the first particle at the origin, and then successively place the succeeding particles randomly within unit balls according to the generating spanning tree. Once we have the position of all particles we check the inter-particle distances to determine if the distances are greater than or less than one, and thus map the configuration to a graph. The volume of the enlarged domain is straightforward to calculate, as each edge of the spanning tree contributes a factor of the volume of the unit ball in D dimensions, which may also be given in terms of B_2 as $(2B_2)^{k-1}$.

The efficiency of the algorithm may be improved by taking in to account all labeled isomorphs of G which may be generated by the spanning tree, but we then must divide by this unlabeling factor to get the correct result.

This method of calculating Ree-Hoover integrals may be extended to calculating the virial coefficient itself, which up to a factor is given by the sum of the Ree-Hoover integrals of all labeled biconnected graphs multiplied by their

star content. Thus we require a set of spanning trees which are able to generate all biconnected graphs, and we also need to calculate the unlabeling factor for each of the biconnected graphs. Ree and Hoover[12,13], Janse van Rensburg[15], and Vlasov et al.[16] proceed by finding a set of spanning trees, and partitioning the biconnected graphs according to which spanning tree will be used to calculate them. This means that if a given spanning tree produces graphs which are not in its set then these configurations are thrown away. We improve on this by combining the unlabeling factors from each of the spanning trees as the sum of the individual unlabeling factors, and never discard a geometric graph that contributes to B_k.

For each iteration of the Monte Carlo calculation we use each of the set of spanning trees to generate a configuration, which is mapped to a graph. If the graph is biconnected then the contribution of this graph, up to an overall factor, is given by the star content multiplied by the number of possible labelings of the graph, divided by the unlabeling factor.

In practice, for each batch we keep a tally of all of the biconnected graphs generated, and only condense this information using the star content and unlabeling factor values to a value for B_k at the end of the loop. For this work we chose a batch size of 10^7 configurations, and uncertainties were calculated using the standard formula

$$\text{Error} = \left[\sum_{j=1}^{q} \frac{(< I_j > - < I >)^2}{q(q-1)} \right]^{\frac{1}{2}} \tag{15}$$

where there are q independent batches with value I_j. All uncertainties given in this paper are equal to one standard deviation, and the number of batches used in the calculation of the virial coefficients in Table 1 are given in Table 5 of Appendix A.

3.2. Graph Theory Notation

Here we define graph theory notation necessary for the description of the calculation of the star content and unlabeling factor of biconnected graphs, as well as the determination of a set of spanning trees sufficient to generate all biconnected graphs of a particular order.

We will use the term subgraph of a graph G to describe graphs with the same vertex set, but with an edge set that is a subset of the edge set of G. We will allow G to be its own subgraph; when excluding this case we will refer to proper subgraphs.

We define $\mathscr{C}_j(G)$ and $\mathscr{B}_j(G)$ to be the set of subgraphs of G with j edges removed which are connected and biconnected respectively. We define the composition of $\mathscr{B}_i$ and $\mathscr{B}_j$ by applying $\mathscr{B}_i$ to each element of the set $\mathscr{B}_j(G)$ and taking

the union of the resulting sets. The end result is exactly $\mathscr{B}_{i+j}(G)$. Thus

$$\mathscr{B}_i \circ \mathscr{B}_j = \mathscr{B}_{i+j} \tag{16}$$

However, if we apply $\mathscr{B}_i$ to each of the $G' \in \mathscr{B}_j(G)$ then we can see that each subgraph in $\mathscr{B}_{i+j}(G)$ is produced exactly $\binom{i+j}{j}$ times. Thus

$$\sum_{G' \in \mathscr{B}_j(G)} |\mathscr{B}_i(G')| = \binom{i+j}{j} |\mathscr{B}_{i+j}(G)| \tag{17}$$

In particular, for $j = 1$,

$$|\mathscr{B}_{i+1}(G)| = \frac{1}{i+1} \sum_{G' \in \mathscr{B}_1(G)} |\mathscr{B}_i(G')| \tag{18}$$

We will define a minimally biconnected graph in analogy to the definition of a tree: a minimally biconnected graph is a graph for which no proper subgraph is biconnected. If we remove any edge from a minimally biconnected graph then the resulting graph will not be biconnected.

An articulation star or clique cut-set of a graph is a proper subset of vertices that is maximally connected, i.e. edges connect each pair of vertices, and whose removal will result in a disconnected graph.

Let CL be an algorithm that takes as input a graph G and defines a relabeling of the vertices of an input graph. Then we will call CL a canonical labeling algorithm if it can be shown that

$$G'_1 = \text{CL}(G_1) \tag{19}$$

$$G'_2 = \text{CL}(G_2) \tag{20}$$

$$G'_1 = G'_2 \Leftrightarrow G_1 \text{ and } G_2 \text{ are isomorphic} \tag{21}$$

Thus, CL converts labeled graphs to unlabeled graphs, and this can, in the appropriate context, greatly reduce the scale of a problem as there are many fewer unlabeled graphs by a factor of approximately $k!$ at order k.

This is an NP-complete problem, and as such it is believed that it is impossible to obtain an algorithm that can be guaranteed to determine the canonical labeling of a graph in polynomial time in the number of vertices k.

An efficient algorithm has been developed by McKay [33] for the purpose of calculating the automorphism group and also the canonical labeling of a graph. Through his own testing on random graphs he finds performance for the canonical labeling procedure is approximately $O(k^\beta)$ with $2 < \beta < 3$ for different classes of graphs despite the fact that this is an NP-complete problem. McKay's implementation of this algorithm in the C programming

language, nauty (no automorphisms, yes?), has been extensively used here.

3.3. Star Content

To calculate the star content of all biconnected nine and ten point graphs, we use the formula of Ree and Hoover[13] outlined in Section 2, here given in the notation of Section 3.2

$$SC(G) = \sum_{i=0}^{|E|} (-1)^i |\mathscr{B}_i(G)| \tag{22}$$

We note that $|\mathscr{B}_0(G)| = 1$ if G is biconnected, and that $|\mathscr{B}_i(G)| = 0$ for $i > 0$ if and only if G is minimally biconnected. Hence we can enumerate all subgraphs with a certain number of edges of a given biconnected graph, if we have this information for the subgraphs. This naturally defines a recursive procedure, where if we apply this enumeration algorithm to the complete star, and recursively apply it to all unlabeled subgraphs, we will generate this list and hence can calculate the star content.

It is more memory efficient, however, to enumerate all subgraphs for graphs with k edges (the Ree-Hoover ring), then to enumerate subgraphs of graphs with $k + 1$ edges, until we finally reach the complete star with $k(k-1)/2$ edges. As a by-product, all minimally biconnected graphs up to tenth order were generated and recorded for use in the spanning tree algorithm of Section 3.4. Using this procedure the star content for all ten point Ree-Hoover graphs was calculated in a matter of 30 minutes. We would therefore expect that the star contents for B_{11} may be calculated in a matter of days, but the problem is significantly more demanding on computer hardware as a large amount of memory is needed to perform the calculation efficiently.

We plot histograms of the number of labeled graphs versus star content for B_6, B_7, B_8, B_9, and B_{10}, in Figures 2–6 of Appendix B. For these figures we exclude graphs with zero star content which have an articulation star, and it is for this reason that the value appears to be low for $k = 6, 7$. For $k \geq 8$ the zero star content value is far greater than the next largest value, and for this reason is not shown in the plots. Note that the histograms become sharply peaked around zero star content, and that these plots become increasingly symmetric as one increases the order.

It is natural that the star contents should be peaked around zero given the constraint imposed by Eq. 9. However, it is not obvious that there should be such a strong symmetry between graphs with star contents of opposite sign, and it would be desirable to find a reason for this behavior.

3.4. Spanning Trees

To find a minimum or close to minimum set of spanning trees we proceed as follows. We take the set of minimally biconnected graphs obtained during the star content calculation procedure.

We then need to enumerate all labeled spanning trees of each of the minimally biconnected graphs, and use nauty to help keep a list of the unlabeled spanning trees of each graph.

The problem of enumerating all spanning trees of a graph is considerably more difficult. If a graph has a large number of spanning trees, then the best available algorithms take time $O(N)$ with sub-leading additive terms, where N is the number of spanning trees. There are many algorithms available which may be distinguished by the sub leading terms, or in the amount of memory required, and by whether they output each of the spanning trees, or output the difference between consecutive trees.

We have implemented an algorithm[34] which uses $O(V + E + VN)$ time and $O(V + E)$ space. As we are only concerned with the case where V is small, the resulting increase in complexity does not matter much.

Naturally, each biconnected graph must have at least one minimally biconnected graph as a subgraph, and thus if we find a set of spanning trees that can generate all minimally biconnected graphs then necessarily we will be able to generate all biconnected graphs.

We could use all spanning trees as our set without any problem. The reason we do not wish to do this in practice is that some graphs such as the ring graph contribute significantly to the final result, but only have perhaps one or two of a large number of spanning trees that will be able to generate it.

We store this information in matrix form as follows: $A_{ij} = 1$ then spanning tree j is a subgraph of minimally biconnected graph i, otherwise $A_{ij} = 0$. As posed, this is the minimum set cover problem, for which no known polynomial time algorithm exists.

The minimum set cover problem may be defined as follows: given a matrix in which all entries have the value of either 0 or 1, and there is at least one 1 in each row, then what are the minimum number of columns that can be chosen such that there is one or more 1's in each row? This problem has been shown to be NP-complete, and the authors could not find implementations of algorithms that are efficient on average for random matrices in the vein of the canonical labeling algorithm of McKay.

However, for our purposes we did not need the exact minimum, and we can apply the greedy algorithm which will produce a minimal set cover (in the sense that we cannot remove any spanning tree from the final result without leaving a graph uncovered), that will be sufficiently close to the minimum for our purposes. The greedy algorithm is defined in the following way: choose the column with

the greatest number of 1s, where if there is a tie we break the tie arbitrarily, then remove that column and the rows which have now been covered. Repeat until there are no rows remaining, at which point the algorithm terminates and returns the numbers of the columns which have been removed. We implemented a slight variation of this: at the beginning of the main loop of the algorithm, if any row has a single 1 then the corresponding column is chosen initially, as it must be included in any set cover solution.

We apply this algorithm to find a near minimum set of spanning trees which are able to generate all biconnected graphs for orders $k = 5, \cdots, 10$, and these are shown in Fig 7 of Appendix C.

We may also optimize the procedure by choosing trees that will minimize the error in the Monte Carlo procedure by efficiently calculating large diagrams. We could do this rigorously, by performing the integration over a range of dimensions and orders, and obtaining a different set of trees for each case. We note here that the Ree-Hoover ring is one of the largest diagrams to the order we calculate, and that the ring diagram and most other loosely packed diagrams can be efficiently generated by the tree without any leaves (it is the only tree required to generate B_5 as can be seen in Fig 7). For this reason we choose to have multiple copies of the tree without any leaves in our set of spanning trees. We have compared this set with the set of all spanning trees and it is more efficient, but we have not performed extensive testing to justify this choice.

We make the comment that there is no difficulty in carrying this procedure out to much higher order, as the number of trees and minimally biconnected graphs grow relatively slowly with order compared with the rate of growth of the total number of graphs.

3.5. Unlabeling Factor

Now that we have our minimal set of spanning trees, we need to calculate the unlabeling factor as defined by Ree and Hoover.

The unlabeling factor is defined as the number of ways in which a given spanning tree may generate a particular labeled graph. Alternatively, we may define it as the number of labeled isomorphs of a particular graph which have the (labeled) spanning tree as a subgraph.

Ree and Hoover[12,13,14], Janse van Rensburg[15], and Vlasov et al[16] proceed by partitioning the set of biconnected graphs in to those which will be calculated by spanning tree 1, 2, 3, etc., and determining the unlabeling factor for each unlabeled graph. This is a computationally intensive procedure in the same manner as for the star content calculation, although not quite as intractable. This is because the number of labeled trees that are subgraphs of the complete star is k^{k-2}. Thus we will need to enumerate approximately $k^{k-2}2^{k(k-1)/2}/k!$ spanning trees, which still grows very fast with order.

We improve on this method in two respects; firstly, we do not partition the graphs, and allow the spanning trees to generate any of the biconnected graphs. In this manner we do not throw out any biconnected configurations that we generate. The combined effect of unlabeling factors from all of the spanning trees is merely the sum of the individual unlabeling factors. Secondly, in this formula we may use any unlabeled spanning tree more than once if we choose. As noted in Secttion 3.4, we use a minimal set of spanning trees but with repetitions of the tree with no leaves.

We then proceed as for the star content, as Eq. 22 applies to the operator for connected graphs $\mathscr{C}_j$, with the difference that we need to keep track of all connected graphs (not just biconnected graphs), and we only need to know the unlabeling factor of each graph rather than the count of subgraphs partitioned by the number of edges they have.

3.6. Details of the Monte Carlo Procedure

All code is written in the C programming language, and the calculation has been compiled and run on Linux machines with Pentium 4 processors.

We use the random number generator of Ziff[35], and in some cases we have confirmed results with the random number generator of Knuth[36].

We generate random points using the algorithm of Banerjia and Dwyer[37] for $D = 3, 4, 5$, and use similar accept or reject algorithms for higher dimension. Alternative methods which do not require the rejection of any generated points, such as using Gaussian variables, may be faster for higher dimensions, but as this is not the bottleneck step in the algorithm we did not implement or test such alternatives.

Given a set of N_{span} spanning trees which will be used to generate configurations, we wish to be able to generate configurations as fast as possible by minimizing the number of random points to generate. To generate each tree we will need to have $k - 1$ random points and hence at first sight we need a total of $(k - 1)N_{\text{span}}$ random points for each iteration. By using the same set of random points for each spanning tree we only need to generate $k - 1$ random points per iteration.

The remaining detail of the Monte Carlo calculation that needs to be discussed is how to identify graphs as they are being generated. The method used was to create a hash table of all canonically labeled biconnected graphs with non-zero star content, so that when a graph is generated one can calculate the canonical label and check if it is in the hash table using linear probing[36]. In practice, the canonical labeling algorithm of McKay[33] is quite slow compared to the speed at which configurations are generated, and so if possible we wish to avoid this step.

For small graphs, which for the computers on which this program was run means for eight or less vertices, we can create an array with $2^{k(k-1)/2}$ elements for

which the address is identified with all labeled graphs of k points. One can map any graph to a sequence of $k(k-1)/2$ bits by imposing an order on all vertex pairs, and then giving the bit corresponding to vertices i and j a value of 1 if $(i, j) \in E$, and 0 otherwise. Thus once a graph is generated the canonical label can be quickly looked up in this array provided some pre-processing is done before the main loop of the Monte Carlo integration. Unfortunately, as the total number of labeled graphs grows extremely rapidly with order, memory limitations mean that even on a supercomputer it would not be possible to do this for graphs with more than 9 vertices.

For large graphs it is therefore much more difficult to perform the identification quickly, and so we attempt to identify if the graph has non-zero star content prior to calculating the canonical label. In particular contributing graphs must be biconnected, and cannot contain an articulation star, as discussed by Ree and Hoover[13]. To this end, a graph that has been generated is first checked to see if there are any vertices of degree 1, and then tested for biconnectivity, and then checked to see if it has an articulation star using an algorithm described below. If any of these conditions are met, then the star content is necessarily zero (although many graphs with zero star content do not have an articulation star); otherwise the canonical label is calculated using the canonical labeling algorithm of McKay[33].

Ree and Hoover[12] showed that graphs with an articulation star will have zero star content, although the converse is not true: some graphs with zero star content have no articulation star for orders greater than 5. An articulation star, otherwise known as a clique separator in the mathematical literature, is a completely connected subset of vertices of a graph whose removal disconnects the graph. A biconnected graph is a graph with no articulation points, and so the set of graphs with no articulation star is a natural generalization. For the purpose of identifying graphs with an articulation star, we implement an algorithm[38,39,40] which finds all articulation stars by finding a minimum ordering of the graph, and calculating the resulting fill-in graph. In practice, we used an algorithm which finds minimal rather than minimum orderings as this is much faster; the trade off is that some graphs with an articulation star will not be identified, but for graphs generated in the calculation of B_9 and B_{10} this occurred only about 2 percent of the time. Note that a graph is never falsely identified as having an articulation star when it does not.

An alternative method would be to implement the algorithm of Whitesides[41] in which a single articulation star is found in the same asymptotic time as all articulation stars are found by the minimal ordering method. However, the method of Whitesides perhaps should be explored as we are interested in small graphs, where the asymptotic behavior of the algorithm is perhaps not as important as the overhead involved in the calculation.

Given the star content, and unlabeling factor, we may then proceed to calculate the virial coefficients up to order ten, in any integer dimension. The results of these computations have been given in Table 1.

4. BACKGROUND

We describe in this section the phase transition undergone by hard spheres in Subsection 4.1, and the rigorous information we have about this system in Subsection 4.2. Ideally, we would like to study the relation of the phase transitions to the virial coefficients. However the unambiguous interpretation of the ratio plots and their relation to the freezing transitions seen in computer studies is made difficult by the fact that we have very few exact results available for the hard sphere system beyond the general theorems that the pressure is continuous and non-increasing for positive densities in the physical region. For this reason in Subsection 4.3 we discuss the various scenarios that have been proposed for the position of the leading singularity of hard spheres in order to provide a framework for later discussion in Section 5.

4.1. Phase Transition

Perhaps the property of hard spheres which is the most interesting and surprising characteristic is the existence of a phase transition, as discovered for $D = 3$ in 1957 by Alder and Wainright[4] via molecular dynamics simulations, and Wood and Jacobson[5] through Monte Carlo methods, and for $D = 2$ via molecular dynamics in 1962 by Alder and Wainright[42]. Wood[43] provided confirmation for the $D = 2$ results using Monte Carlo methods in 1968. For dimensions three, four and five[44] the phase transition is believed to be first order, while for hard discs the situation is more controversial despite intense research efforts over the past forty years[42,45,46,47]. Recently Jaster[48] showed that as the density of the system increases that hard discs first undergo a first or second order transition from the fluid phase to a hexatic phase with short range positional and quasi long range orientational order, and then undergo another second order transition to the solid phase which has quasi long range positional and orientational order. This is consistent with the Kosterlitz–Thouless–Halperin–Nelson–Young scenario, for which both transitions must be second order.

The phase transition freezing (ρ_f) and melting (ρ_s) densities are given in Table III for $D = 2$ [45,48], $D = 3$ [4,49,50], and $D = 4, 5$ [44]. We list also the density ρ_{cp} and the scaled density $B_2\rho_{cp} = 2^{D-1}\eta_{cp}$ of the densest lattices for dimensions $D = 2, \ldots, 8$ from the lattice catalogue of Nebe and Sloane[51]. Note that the density $\eta = 1$ corresponds to all space being filled. Finally, we include the lower bound of the radius of convergence obtained by Lebowitz and Penrose[52].

Table III. Values for B_2, the density of the closest packed lattices, the densities at which freezing (ρ_f) and melting (ρ_s) occur, and the bound of Lebowitz and Penrose[52], for hard spheres of diameter σ in dimensions $D = 2, \cdots, 8$

D	B_2	ρ_{cp}	$B_2\rho_{cp} =$ $2^{D-1}\eta_{cp}$	ρ_f/ρ_{cp}	ρ_s/ρ_{cp}	ρ_{LP}/ρ_{cp}
2	$\frac{\pi\sigma^2}{2}$	$\frac{2}{\sqrt{3}\sigma^2}$	$1.8137\cdots$	0.78	0.81	0.03990
3	$\frac{2\pi\sigma^3}{3}$	$\frac{\sqrt{2}}{\sigma^3}$	$2.9619\cdots$	0.66	0.75	0.02444
4	$\frac{\pi^2\sigma^4}{4}$	$\frac{2}{\sigma^4}$	$4.9348\cdots$	0.50	0.68	0.01467
5	$\frac{4\pi^2\sigma^5}{15}$	$\frac{2\sqrt{2}}{\sigma^5}$	$7.4441\cdots$	0.41	0.62	0.00971
6	$\frac{\pi^3\sigma^6}{12}$	$\frac{8}{\sqrt{3}\sigma^6}$	$11.9343\cdots$			0.00605
7	$\frac{8\pi^3\sigma^7}{105}$	$\frac{8}{\sigma^7}$	$18.8990\cdots$			0.00382
8	$\frac{\pi^4\sigma^8}{48}$	$\frac{16}{\sigma^8}$	$32.4696\cdots$			0.00224

The existence of singularities for $D \geq 3$ at ρ_f and ρ_s is much more controversial than the singularities for $D = 2$. It has long been argued by Fisher[53] that at these phase boundaries the pressure will be infinitely differentiable but will not be analytic and thus cannot be analytically continued into the region $\rho_f < \rho < \rho_s$ from either side. These singularities have been proven to exist in the Ising model by Isakov[54], but for hard spheres nothing rigorous has been proven. In this scenario the freezing density ρ_f can be determined in principle from the leading singularity on the positive real axis of the low density equation of state.

The alternative view of the first order (freezing) transition in hard spheres for $D \geq 3$ is the assumption that there are no singularities at the phase boundaries and that analytic continuation from both sides is possible. The freezing transition is seen as a Maxwell construction making a convex envelope from a low and a separate high density free energy. In this scenario it is impossible to determine the freezing density from the low density equation of state alone.

It is obviously of great theoretical importance to determine which of these two scenarios is correct for hard sphere for $D \geq 3$. This is a particularly difficult question if the radius of convergence of the virial series is determined by a singularity in the complex plane, which the ratio plots indicate is very likely the case for $D \geq 4$. In this case if the radius of convergence is less than the freezing density ρ_f it is necessary to find a way to analytically continue the virial expansion beyond the radius of convergence to study a possible singularity at ρ_f. It is surely not possible to extract from our 10 term series both a leading singularity in the complex plane and to reliably continue the expansion beyond the radius of convergence to detect an infinitely differentiable singularity at ρ_f. Consequently we will restrict our attention to locating the leading singularity in the complex plane.

4.2. Rigorous Results

There are few rigorous results available for the problem of hard spheres, and we will briefly summarize those few results here.

Groeneveld[55] proved that for the cluster expansion the radius of convergence must be greater than $1/(2eB_2)$, where $e = 2.71828\cdots$, and less than $1/(2B_2)$. In addition, it is known that the cluster coefficients alternate in sign and hence the leading singularity is on the negative, real fugacity axis. Lebowitz and Penrose[52] adapted this bound to derive a corresponding expression for the virial series, given in Eq. 23.

$$\rho_{LP} \geq \frac{0.14476}{2B_2}$$

$$\eta_{LP} \geq \frac{0.14476}{2^D} \tag{23}$$

Thus we know that the pressure is an analytic function of density for small densities; unfortunately in practice this bound does not seem to be close to the true radius of convergence as it is a long way from the density at which the phase transition is seen to occur, as can be seen from Table III.

Later Fisher[56] obtained bounds on the pressure in the vicinity of close packing for a D–dimensional system of hard particles. Extending the results of Hoover[57] for hard parallel cubes, Fisher was able to prove that for $\Upsilon \equiv \frac{\rho_{cp}}{\rho} - 1 \rightarrow 0$ that

$$\frac{\xi_1 D}{\Upsilon} \leq \frac{P}{\rho k_B T} \leq \frac{\xi_2 D}{\Upsilon} \tag{24}$$

where $0 < \xi_1 < 1 < \xi_2 < \infty$. For the general case of hard core particles, which includes hard spheres, he was able to establish the weaker relation

$$\eta_1 \ln \Upsilon^{-1} \leq \frac{P}{\rho k_B T} \leq \frac{\eta_2 \ln \Upsilon^{-1}}{\Upsilon} \tag{25}$$

for any $\eta_1 < 1 < \eta_2$.

4.3. Scenarios for the Position of the Leading Singularity

We present here various scenarios that exist for the location and nature of the leading singularity of the virial series for hard spheres in D dimensions.

Over the past 40 years many approximate equations of state have been proposed for hard spheres, most commonly for the case $D = 3$. These approximates may be categorized by the location of their leading singularity.

Many have high order poles at the space filling density $\eta = 1$, including the solutions of the compressibility and virial Percus–Yevick integral equations[31] for

$D = 3$ by Thiele[58] and Wertheim[59,60], the scaled particle theory of Reiss, Frisch, and Lebowitz[61], a proposal by Guggenheim[62], and the widely used empirical formula of Carnahan and Starling[63].

The equations of state of Goldman and White[64] and Hoste and Dael[65] have simple poles at or near the packing fraction of closest packed hard spheres.

Other equations of state have a fractional power law divergence at or near the "random close packed" density $\eta_{rcp} = 0.64$ as defined by[66,67,68,69]. These approximates are obtained by constraining the divergence of the leading singularity to be of the form

$$Pv/k_B T = A(\eta - \eta_{rcp})^{-s} \tag{26}$$

As an example s is estimated as 1 in[70] as 0.678 in[71] and 0.76 in[72]. In[73] other values of η_{rcp} are chosen and the values of s lie in the range $0.6 \leq s \leq 0.9$ depending on the approximation used.

Some approximate equations of state include the freezing density, and we mention in particular that Torquato [74,75] proposes an equation of state which agrees with the equation of Carnahan and Starling[63] for $\eta < \eta_f$ but which is of a different form for $\eta > \eta_f$.

For dimensions greater than 3, we note the analytic solution of the Percus–Yevick equation in $D = 5$ obtained independently by Freasier and Isbister[76] and Leutheusser[77], as well as the recent work of Robles, López de Haro, and Santos[78], in which the analytic solution was obtained for the Percus–Yevick equation in $D = 7$. One of the most interesting results is that the radius of convergence is no longer determined by the singularity on the positive real axis at $\eta = 1$, but instead by a singularity on the negative real axis for $D \geq 5$.

Baram and Luban[79] in 1979 fitted the first seven virial coefficients using Levin approximants, and concluded that the leading singularity is at the close packed density.

More recently, in 1994 Sanchez[80] fitted the virial series with a Padé approximant, and then expressed the density in terms of the compression factor by inverting the series. He then fitted the inverted series with Padé approximants of increasing order to obtain estimates of the density at which the compression factor diverges. Sanchez then argued that as the order of the Padé approximants was increased that the position of the leading singularity converged to the density of close packing in two and three dimensions, and this was taken as evidence that the leading singularity of the virial series is in fact the density of closest packing.

Gaunt and Joyce[81] provided a counter argument to the conclusion and methods of Baram and Luban, and indeed to Sanchez despite the fact that the work of Sanchez came well after. They performed a ratio analysis[82] of the virial series, which they advocated as a robust method in the absence of any knowledge of the exact form of the function being described by the series. What was then the seven

term virial series appeared to be behaving smoothly and ratio analysis suggested that the leading singularity lies on the positive real axis, perhaps at the space filling density. However, they pointed out that there is good reason to be cautious in extracting asymptotic behavior from only the low order coefficients: for several varieties of lattice gas with either nearest neighbor exclusion or first and second nearest neighbor exclusion, they show that the ratios initially behave smoothly indicating a singularity on the positive real axis, and then suddenly change behavior, and eventually change sign. This is because the asymptotic behavior is determined by a complex conjugate pair of singularities that mask the physical singularity on the real axis.

The only relevant models which demonstrate a phase transition for which exact results are available are hard core lattice gases in two dimensions. In particular the hard hexagon model[83,84,85] and a model of hard squares[86] have been exactly solved, and in both cases the radius of convergence is limited by a complex conjugate pair of singularities thus resulting in virial coefficients that oscillate in sign.

Other relevant models include that of hard parallel cubes[87] for which negative virial coefficients have been seen as low as sixth order, along with the Gaussian model[28,88,89] for which negative coefficients can be seen for dimensions $D \geq 1$. In particular for the Gaussian model oscillations are seen in the sign of the virial coefficients and this is evidence that the dominant singularities to are in the complex plane.

Virial coefficients have been calculated for hard ellipsoids and other hard particles in two and three dimensions[16]. For these models we also see negative coefficients at relatively low order, with the effect being more dramatic for shapes which are far from spherically symmetric; in the case of ellipsoids, the effect is dramatic for large aspect ratio.

The phase transition behavior of hard core systems ultimately depends on the geometry of the crystalline phase. Thus it is not immediately obvious how relevant hard hexagons and hard parallel cubes are to the hard sphere problem, as the crystalline phase fills all space and the phase transition has been observed to be second rather than first order. However, one could argue that this is only important in the vicinity of the phase transition itself, and that the leading singularities of the virial series for $D \geq 2$ may be a conjugate pair of singularities in the complex plane.

5. DISCUSSION

The most important property of the virial coefficients B_k is not their actual numerical values for k less that some finite number but rather their asymptotic behavior as $k \to \infty$ because it is the asymptotic value which determines the radius of convergence. Of course no finite number of virial coefficients can give information on the $k \to \infty$ behavior unless there is some *a priori* reason to expect that the values of k are already in the asymptotic $k \to \infty$ regime.

In Subsection 5.1 we propose two such criteria for the asymptotic regime of hard spheres and will see that for $k \leq 10$ there is no dimension in which both criteria are fully satisfied. Nevertheless it is still of interest to determine what results are obtained if well known methods are used in an attempt to determine the asymptotic behavior of the series from the first ten virial coefficients. In Subsections 5.2 and 5.3 we proceed with the methods of ratio analysis and of differential approximants respectively as robust and general methods for the purpose of series analysis.

5.1. Criteria for Asymptotic Behavior of B_k

Classical systems of hard particles for which the interaction potential is either infinite or zero, such as hard spheres and parallel hard cubes, are special in that some graphs have Ree-Hoover integrals which are identically zero for dimensions D less than some maximum value, as the restrictions imposed by the graph are so many that no configuration of points may satisfy them. Hence the number of Ree-Hoover integrals contributing at a particular order depends on dimension. We study this problem by performing the Monte Carlo calculation outlined previously, but in addition we keep track of how many diagrams have been generated at least once from batch to batch whereas for the numerical calculation of B_k this information was discarded.

We tabulate our results for the number of contributing Ree-Hoover integrals in Table II. For $D = 1$, only the complete star graph is non-zero, for $D = 2$ many graphs are zero at the orders calculated, but for $D > 2$ it is difficult to make any estimate of how many zero diagrams there are. This is because there are a large number of graphs with numerically small Ree-Hoover integrals, and we do not know of any method to estimate the distribution function for the values of these small diagrams. Without this information it is impossible to estimate the number of zero diagrams until the Monte Carlo procedure has run for a sufficiently long time such that almost all non-zero diagrams have been generated. It was found to be impossible to reach this regime for B_9 and B_{10} in dimensions $D = 3, 4$, and hence we suggest that new direct ways must be found to count zero diagrams if progress is to made on this problem for dimensions greater than two.

The rate of growth of the number of non-zero Ree-Hoover integrals in two dimensions is far less than that of the number of biconnected graphs with non-zero star content. It is possible that the rate of growth has been reduced from $2^{k(k-1)/2}$ to something like exponential growth, but there is not enough data to make a definitive statement on this issue.

Criterion 1
The number of nonzero Ree Hoover diagrams has approached its large k behavior.

For $k = 10$ this criterion is only completely fulfilled for $D = 2$ and is not fulfilled at all for $D \geq 5$.

Our second criterion has been presented in our previous paper [27]

Criterion 2
The loose packed diagrams with the number of $\tilde{f}$ bonds near their maximum value numerically dominate B_k.

The validity of this criterion has been studied in detail in [27]. Here it was seen that for $D = 3$ and $k \geq 12$ the criterion is well satisfied and that as D increases the criterion is satisfied for smaller values of k. However, for $D = 2$ the criterion was not satisfied even for k as large as 18.

We thus conclude that there is no dimension in which both of these criteria are fully fulfilled although for $D = 3$ and $D = 4$ it is possible that they both could hold for some moderate values of k of the order of 12 to 14.

5.2. Ratio Analysis

We begin our analysis of the virial coefficients given in Table I by making a ratio analysis[81,82]. By comparison with the test function

$$\sum_{k=1}^{\infty} a_k z^k \quad \text{with} \ a_k = k^s/z_c^k, \tag{27}$$

which as $z \to z_c$ has the singularity

$$(1 - z/z_c)^{-1-s}, \tag{28}$$

we see, up to possible logarithms which cannot possibly be seen in our ten term series, that the $k \to \infty$ behavior of the ratios

$$a_{k+1}/a_k \sim z_c^{-1}(1 + s/n + O(n^{-2})) \tag{29}$$

indicates a simple pole at $z = z_c$ if $s = 0$ and a divergence more (less) singular than a pole if s is positive (negative). Note in particular that if $s < -1$ then the function is finite at $z = z_c$ and if $s < -1 - n$ the first n derivatives are also finite at $z = z_c$ even though there is a divergence in the $(n + 1)^{st}$ derivative.

We normalize the ratios to the density of the closest packed lattice by plotting $B_k \rho_{cp}/B_{k-1}$ and these ratios are plotted versus $1/k$ in Figures 8–12 for $D = 2, \cdots, 8$. The values of ρ_{cp} obtained from the catalogue of lattice packings of Nebe and Sloane [51] are given in Table III.

The qualitative description of our results is as follows.

5.2.1. $D = 2$

The plot of $B_k \rho_{cp}/B_{k-1}$ for $D = 2$ is given in Fig 8. The ratios are all positive and are smoothly decreasing. At $k = 10$ the ratio is 0.9992 which is just less than the value of unity it would have if the leading singularity were at close packing. However, the ratios are still falling and hence suggest the radius of convergence is determined by a singularity at a density greater than close packing. For comparison the ratios for $D = 3$ are also plotted.

5.2.2. $D \geq 5$

The ratios for $D \geq 5$ are plotted in Figures 9 and 10. In these cases the first few virial coefficients are positive (giving positive ratios) and then to the order given the coefficients alternate in sign (giving negative ratios). This suggests that there is a singularity on the positive real axis which dominates the series initially, but there is a second singularity in the complex plane or negative real axis which is closer to the origin which determines the actual radius of convergence and dominates the ratios at high order. If the leading singularity is on the negative real axis the ratios will smoothly converge to some negative value, otherwise the ratios will oscillate.

5.2.3. $D = 4$

The ratios for $D = 4$ are plotted in Fig 11. There are no negative virial coefficients for $k \leq 10$ but even though the accuracy for B_{10} is limited there seems to be a very definite oscillation which is developing just as oscillations develop for $D \geq 5$. Hence, from examining Fig 11 we expect that negative virial coefficients will occur for k not much greater than 12.

5.2.4. $D = 3$

The most important case is $D = 3$ and this is also the most difficult to interpret. This case is plotted in Fig 9 where it is compared with with $D = 2$ and is plotted on an expanded scale in Fig 12. In the plot of Fig 9 the ratios for $D = 3$ appear much the same as the ratios for $D = 2$ and extrapolate to a density significantly larger than ρ_{cp}. However, an inspection of Fig 12 reveals that unlike the situation for $D = 2$ the ratio plots for $D = 3$ are not always convex and can be seen from the magnitude of the slopes of the line segments given by $5.8959 \cdots$, 4.43686(21), 2.80402(85), 2.212(32), 2.279(15), 1.745(75), and 1.34(34). This lack of monotonicity is evidence that the ratios for $D = 3$ are displaying small oscillations in amplitude. If these oscillations grow in magnitude then may be expected that eventually there will be oscillations in the signs of the

virial coefficients and the radius if convergence will be determined by a singularity away from the positive real axis.

5.3. Pade and Differential Approximants

5.3.1. Notation

The simplest way to make extrapolations of a finite number of terms in a power series expansion is the Padé approximant which assumes that the power series represents a rational function f(z) expressed as

$$f(z) = \frac{P_M(z)}{Q_N(z)} \tag{30}$$

where $P_M(z)$ and $Q_N(z)$ are polynomials of degree M and N respectively. We refer to this approximant as $[M/N]$. The coefficients of these polynomials are easily computed from the power series of $M + N - 1$ terms by solving a system of linear equations This form cannot possibly represent a pressure which is continuous at its leading singularity and thus is not appropriate for investigating the question of equations singularities in equations of state for the fluid phase of any system. Nevertheless Padé approximant have been used by many authors[12,14,15] either to obtain information about the singularities of the virial series or as approximate equations of state for hard spheres. For reasons of comparison with the literature we list several Padé approximants for $D = 2, 3$ in the text below.

A much more general method for extracting information from power series are the differential approximants presented in detail by Guttmann[82] and references therein including Guttmann and Joyce[90], Joyce and Guttmann[91], Hunter and Baker[92,93] and Fisher and Au-Yang[94]. In this method the power series is assumed to be represented by a function $f(z)$ which is the solution of the linear differential equation

$$\sum_{i=0}^{K} Q_i(z; L_i) \left(z \frac{d}{dz} \right)^i f(z) = R(z; M). \tag{31}$$

where $Q_i(z; L_i)$ and $R(z; M)$ are polynomials of degrees L_i and M respectively

$$Q_i(z; L_i) = \sum_{k=0}^{L_i} q_{ki} z^k, \quad R(z; M) = \sum_{k=0}^{M} r_k z^k \tag{32}$$

This form will incorporate the feature that $P(\rho)/k_B T = \rho + O(\rho^2)$ for $z \to 0$ by requiring that

$$r_0 = 0, \quad \text{and} \quad r_1 = q_{0,1} + q_{0,0} \tag{33}$$

The form (31) is sufficiently general that it allows algebraic (or possibly logarithmic) singularities at the L_K zeros z_j of $Q_K(z; L_K)$ The behavior near these zeroes $f(z)$ in the case where the zeros are simple is

$$f(z) \sim A(z_i)|z - z_i|^{\alpha_i} + \frac{R(z_i; M)}{Q_0(z_i; L_0)} \tag{34}$$

with

$$\alpha_i = K - 1 - \frac{Q_{K-1}(z_i; L_{K-1})}{z_i Q'_K(z_i; L_K)} \tag{35}$$

The special case $K = 1$ and $R(z, M) = 0$ is called a Dlog Padé approximant and in this case $f(z)$ is explicitly given as

$$f(z) = z \exp\left\{-\int_0^z dz \frac{Q_0(z; L_0) + Q_1(z; L_1)}{z Q_1(z; L_1)}\right\} \tag{36}$$

which near the zeroes z_i of $Q_1(z; L_1)$ behaves as

$$f(z) \sim A(z_i)|z - z_j|^{-\frac{Q_0(z_j; L_0)}{z_i Q'_1(z_i; L_1)}}. \tag{37}$$

This $f(z)$ either diverges or vanishes at the singular points z_i and thus, like the Padé approximant the Dlog Padé is not able to accurately represent a singularity in the pressure at a point such as the freezing transition where the pressure is continuous. However, it should be adequate to study the question of whether for $D = 3$ the leading singularity is in the complex plane off the positive real axis.

5.3.2. Method

We fitted the series with regular Padé, Dlog Padé and differential approximants, and attempted to get some measure of how well these approximants represented the series by seeing how effective they were at "predicting" coefficients when given a shortened series. This was done systematically by evaluating a measure which would quantify the relative mean square deviation of predicted coefficients from the actual coefficients of Table I. We reached the conclusion that there was no difference between Padé, Dlog Padé and differential approximants in extrapolating the virial series for hard spheres given the coefficients $B_1, \cdots, B_9$.

The Fortran program NEWGRQD given by Guttmann[82] was used to determine the differential approximants. We will now discuss the information that can be drawn from the approximants in each dimension in terms of the leading singularities, expected asymptotic behavior, and predicted coefficients.

The scatter in the position and exponent of singularities, and in predicted coefficients comes from two sources: uncertainties in the virial coefficients, and differences between the approximants themselves. We take in to account the virial coefficient uncertainties by generating a reasonably large set (1000) of series by

sampling from Gaussian distributions with the center given by the best values listed in Table I, and the width given by the corresponding uncertainties. We then determine the Padé and differential approximants corresponding to each of these series, and combine the results to get mean values with uncertainties for the predicted coefficients of each approximant. In addition we obtain uncertainties for the coefficients of the rational function $P_L(\rho)/Q_M(\rho)$ for the Padé approximants. We found that the scatter in the predicted series coefficients due to uncertainties for Padé approximants matched the scatter among different approximants quite closely. The differential approximants were considerably more sensitive to the uncertainty of the coefficients, and generally were stable for around 2 to 3 less coefficients than the Padé approximants. Below we will neglect the discussion of scatter due to uncertainties in the coefficients and only consider the scatter between approximants.

We list the singularities and corresponding exponents for the differential approximants for $D = 2, 3$ in Tables 6 and 7 of Appendix E, and the singularities and residues of the Padé approximants for $D = 2, 3$ in Tables 8 and 9 of Appendix F. Padé approximants are of little use in determining the singularities of a series unless we have reason to expect the series to be well represented by a rational function. As we have no reason to expect this to be the case for the virial series of hard spheres we do not make reference to these tables below, but include them for the interested reader to compare with the work of other authors[12,14,15,80]. We have not included tables for $D = 4, \cdots, 8$ for reasons of length, and feel that the brief summary we make of the information in each of the tables is sufficient. The dedicated reader may obtain the tables for singularities and exponents/residues in all dimensions, as well as tables of coefficients predicted by the approximants, either by downloading them[95] or upon request from the authors.

Some care needs to be taken in interpreting the tables of singularities and exponents from the differential approximants, and we now discuss some of the relevant issues. Defective approximants, which have a singularity with an anomalously small exponent are marked with the symbol †, and are somewhat arbitrarily chosen as it is not possible to rigorously define what is an anomalously small exponent. We use the *ad hoc* procedure of Hunter and Baker[92], outlined by Guttmann[82], that approximants be deemed defective if they have a pole with residue less than 0.003 that lies approximately inside the radius of convergence of the series. Defective approximants should be avoided as they are really lower order approximants in disguise, with an extra factor from a denominator pole and zero in the numerator that almost cancel. One other observation that should be made is that we expect in general if a series in the variable z has a singularity z_c with exponent α, then the approximants may be expected to determine z_c with more accuracy than α. Thus we expect more scatter between approximants in exponent values than in the position of singularities. In particular, even though we make an observation below about the position of the leading singularity in Table 7 for $D = 3$, nothing can be

said about the exponent. Further evidence for the unreliability of the exponents comes in the form of the large imaginary part of many of the exponents, which is very unlikely to be a true feature of the series. See Guttmann[82] for a much deeper discussion on both of the issues raised above.

We have combined the coefficients predicted by the various approximants[95] to produce Table IV of predicted coefficients for dimensions $D = 2, \cdots, 8$. We discuss these predicted coefficients as well as information obtained about singularities from the differential approximants for dimensions $D = 2, \cdots, 8$ below.

5.3.3. Analysis

For $D = 2$, the leading singularities of the differential approximants lie on the positive real axis with the exceptions of [3, 3; 1] and [3, 2, 2; 0]. In most cases the singularity is located close to $B_2\rho = 1.98$, with an exponent of $-1.74(3)$. We list the singularities of the approximants in Table VI of Appendix E. To make this estimate we have looked at all approximants which were not defective that use all 10 terms in the series, and calculated an average value. We discarded the values from the approximant [2, 2, 2; 0] which appeared to be an outlier. No other singularities follow a consistent pattern, and thus we see no signs of singularities that could eventually lead to sign changes in the virial series. As can be seen[95], predicted coefficients are stable to B_{18}, and are listed in Table IV where the scatter in the predicted coefficient is in the last digit. The Padé approximants [4/5] and [5/4] may be used as approximate equations of state at low density, and although they may be obtained directly from the data we include them for reference purposes along with the compilation of tables[95].

$$f_{[4/5]}(\rho) =$$

$$\frac{1 + 0.699392(B_2\rho) - 0.330330(B_2\rho)^2 + 0.112944(B_2\rho)^3 - 0.0123206(B_2\rho)^4}{1 - 0.300608(B_2\rho) - 0.811727(B_2\rho)^2 + 0.627516(B_2\rho)^3 - 0.178626(B_2\rho)^4 + 0.0213592(B_2\rho)^5} \tag{38}$$

$$f_{[5/4]}(\rho) =$$

$$\frac{1 - 0.0628945(B_2\rho) + 0.138515(B_2\rho)^2 + 0.00676994(B_2\rho)^3 + 0.00399421(B_2\rho)^4 + 0.000477608(B_2\rho)^5}{1 - 1.06290(B_2\rho) + 0.419405(B_2\rho)^2 - 0.113679(B_2\rho)^3 + 0.0218465(B_2\rho)^4} \tag{39}$$

The variation in the polynomial coefficients in these approximants when one takes in to account the uncertainty in the virial coefficients is of the same order as the coefficients themselves. Hence one should not ascribe too much importance to the exact value of the Padé coefficients as they will change as future improvements are made in the accuracy of the virial coefficients.

For $D = 3$, the position of the leading singularity varies more than for $D = 2$: in most cases the leading singularities for the high order differential approximants are in the complex plane with negative real part. However, the position and nature

Table IV. Predicted coefficients for approximants with 10 exact coefficients in dimensions $D = 2, \cdots, 8$, with uncertainty in the last digit. The entry is left blank when it is not possible to even determine the sign of the predicted coefficient.

				Predicted coefficients				
D	B_{11}/B_2^{10}	B_{12}/B_2^{11}	B_{13}/B_2^{12}	B_{14}/B_2^{13}	B_{15}/B_2^{14}	B_{16}/B_2^{15}	B_{17}/B_2^{16}	B_{18}/B_2^{17}
2	1.089×10^{-2}	5.90×10^{-3}	3.18×10^{-3}	1.70×10^{-3}	9.10×10^{-4}	4.84×10^{-4}	2.56×10^{-4}	1.36×10^{-4}
3	1.22×10^{-4}	3.64×10^{-5}	1.08×10^{-5}	3.2×10^{-6}	9.2×10^{-7}	2.6×10^{-7}		
4	1.2×10^{-6}							
5	3×10^{-5}	-4×10^{-5}						
6	4.32×10^{-4}	-3.68×10^{-4}	3.2×10^{-4}	-2.9×10^{-4}	2.7×10^{-4}	-2.5×10^{-4}	1.8×10^{-3}	-2.1×10^{-3}
7	1.43×10^{-3}	-1.40×10^{-3}	1.42×10^{-3}	-1.45×10^{-3}	1.5×10^{-3}	-1.6×10^{-3}	5.5×10^{-3}	-6×10^{-3}
8	2.56×10^{-3}	-2.72×10^{-3}	2.97×10^{-3}	-3.4×10^{-3}	4.0×10^{-3}	-4.4×10^{-3}		

of this singularity varies substantially between approximants, and it is not possible to make a definitive statement as to whether this is a true singularity of the series, or an artifact of the approximant method. For approximants which only allow for 2 singular points, the leading singularity is on the real axis, and may be positive or negative. There does however appear in all approximants to be a stable singularity on the positive real axis, which is generally not the leading singularity. It is located at $B_2\rho = 3.75(3)$, with an exponent of $-2.10(8)$, with the estimate made from all high order, non-defective differential approximants in Table 7 of Appendix E. In accordance with the discussion of Subsection 5.2 this is the singularity that dominates the series initially. If the complex conjugate pair of singularities are indeed the leading singularities of the series then this will eventually lead to a change in sign of the virial series in 3 dimensions. This can be confirmed or rejected by calculating more coefficients, and possibly by increasing the accuracy of the coefficients to B_{10} which may reduce the scatter in the position of the singularities. As can be seen[95], predicted coefficients are stable to B_{16}, and estimates of their values are given in Table 4. We explicitly give here the Padé approximants [4/5] and [5/4] which may be used as approximate equations of state at low density.

$$f_{[4/5]}(\rho) =$$

$$\frac{1 + 0.50999(B_2\rho) + 0.20875(B_2\rho)^2 + 0.036450(B_2\rho)^3 + 0.0035176(B_2\rho)^4}{1 - 0.49001(B_2\rho) + 0.073759(B_2\rho)^2 - 0.018002(B_2\rho)^3 + 0.0057762(B_2\rho)^4 - 0.00054759(B_2\rho)^5} \quad (40)$$

$$f_{[5/4]}(\rho) =$$

$$\frac{1 + 0.80409(B_2\rho) + 0.46662(B_2\rho)^2 + 0.14198(B_2\rho)^3 + 0.029739(B_2\rho)^4 + 0.0028192(B_2\rho)^5}{1 - 0.19591(B_2\rho) + 0.037534(B_2\rho)^2 - 0.060058(B_2\rho)^3 + 0.012303(B_2\rho)^4} \quad (41)$$

As is the case for $D = 2$, if one takes in to account the uncertainty of the virial coefficients then the variance of the coefficients in the Padé approximants is of the same order as the coefficients themselves.

In $D = 4$ there is no clear behavior for the leading singularity that can be gleaned from the approximants; there are cases where the singularity is on the positive real axis, on the negative real axis, or in the complex plane. Predicted coefficients are correspondingly variable, and this may be attributed to the low magnitude and correspondingly poor accuracy of B_9 and especially B_{10}. Almost all approximants predict that B_{11} will be positive (see Table 4), but after that the predictions diverge: some allow for negative coefficients as soon as B_{12}, and many allow for negative B_{13} or B_{14}, but this is in no way an improvement on our qualitatively based prediction in Subsection 5.2 that we will soon see negative coefficients for $D = 4$. Higher order virial coefficients and better accuracy for the known virial coefficients will help to resolve this question.

For $D = 5$ the approximants give no clue as to the position or nature of the leading singularity. Predicted coefficients are stable only to B_{12}, and are given in Table 4. Some approximants predict negative coefficients for B_{13}, and there are no predictions of asymptotic behavior that are consistent between the different approximants.

We will discuss the cases of $D = 6, 7, 8$ together, as they are all very similar. The leading singularity is generally on the negative real axis, which suggests that the alternation in sign of the virial coefficients will continue for higher orders. There is no apparent pattern in the position of the next to leading singularity. Predicted coefficients are stable to B_{16} for $D = 6$, and to B_{18} for $D = 7, 8$. This behavior is consistent with either the leading singularity being on the negative real axis as the differential approximant analysis suggests, or that there are complex conjugate singularities adjacent to the negative real axis but close enough so that their position cannot be accurately determined with ten virial coefficients.

6. CONCLUSION

The key result is that negative virial coefficients have been found for $D \geq 5$, and a strong signal was found via the method of ratio analysis in Subsection 5.2 that negative coefficients will soon occur for $D = 4$. On the basis of evidence from the methods of ratio analysis in Subsection 5.2 and differential approximants in Subsection 5.3 there is a distinct possibility that at higher order some virial coefficients for $D = 3$ will be negative. This would contradict the frequent assumption that all virial coefficients are positive for hard spheres in three dimensions. More work needs to be done to confirm or reject this hypothesis; in particular the calculation of B_{11} and possibly B_{12} may provide the necessary evidence. For $D = 2$ no deviation is seen from the behavior of a series that is dominated by a singularity on the positive axis at a density close to the space filling density. However, as discussed in Subsection 5.1, unless there is good reason to believe that the series has entered the asymptotic regime then it is impossible to draw strong conclusions about the position and nature of the leading singularity.

ACKNOWLEDGMENTS

A NUMBER OF CONFIGURATIONS

Numerical results for the virial coefficients are to be found in Table I. We list the number of batches of 10^7 configurations in Table V. The total number

Table V. Number of batches of 10^7 configurations used in virial coefficient calculations, as a function of order and dimension

D	B_4/B_2^3	B_5/B_2^4	B_6/B_2^5	B_7/B_2^6	B_8/B_2^7	B_9/B_2^8	B_{10}/B_2^9
2	1000	9625	9000	9000	15384	19553	6149
3	1000	52573	53463	63751	64675	87609	151349
4	1000	8454	9400	10299	21400	31903	38699
5	23199	8436	8618	8597	15607	21042	15398
6	1000	8423	8600	8542	5899	6300	1229
7	23010	8213	8600	8500	5898	6300	1300
8	1000	8209	8500	8493	5763	6265	1300

of configurations can be obtained by multiplying the number of batches by the number of spanning trees used at a particular order.

B STAR CONTENT RESULTS

Here we plot histograms of the star content for labeled graphs contributing to B_6, B_7, B_8, B_9, and B_{10}.
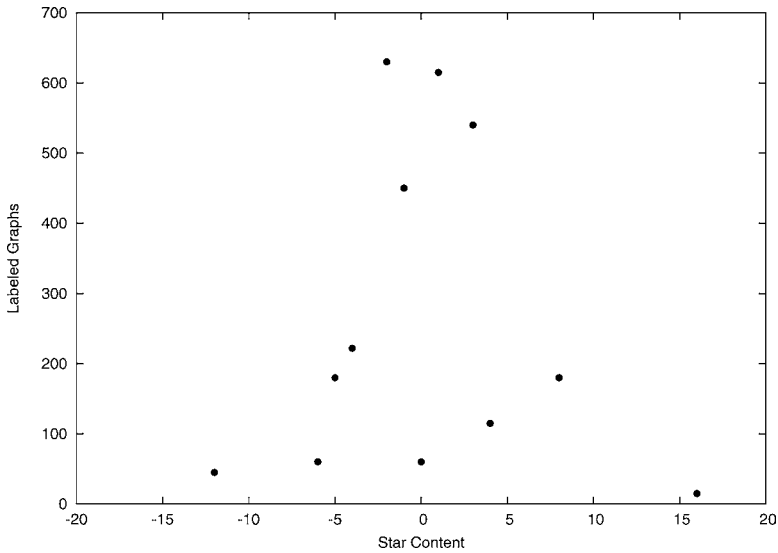

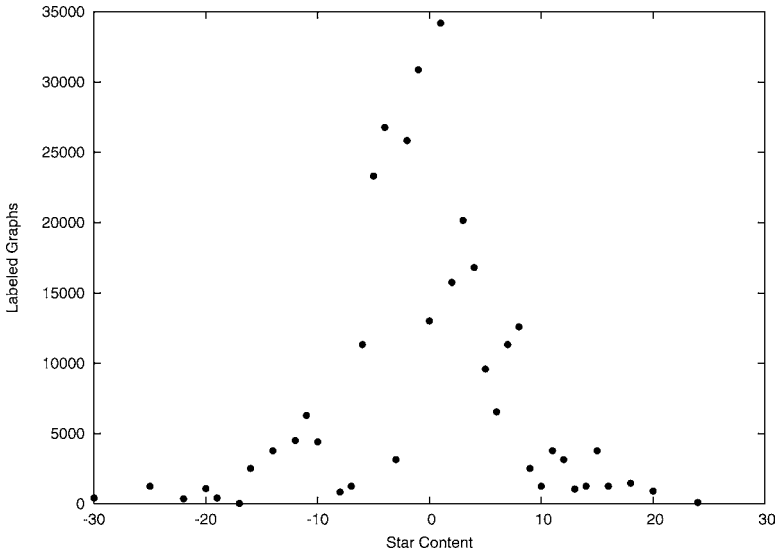**Fig. 2.** Histogram plot of number of labeled graphs versus star content for B_6.

Fig. 3. Histogram plot of number of labeled graphs versus star content for B_7.
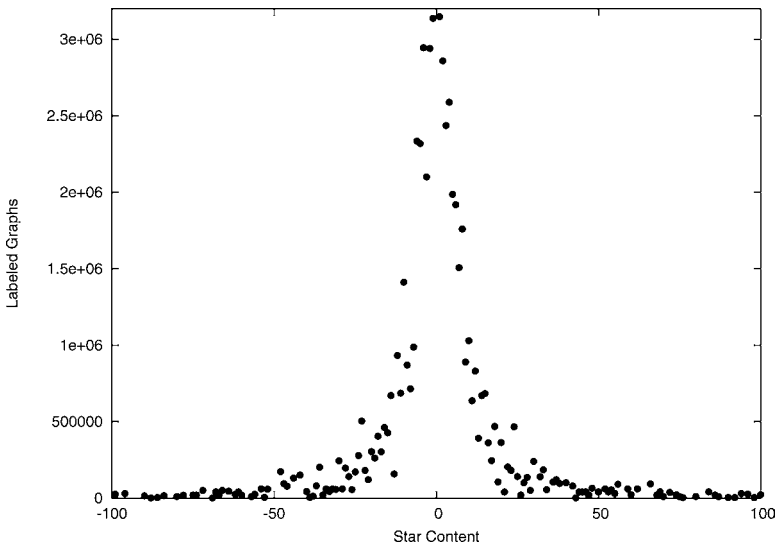

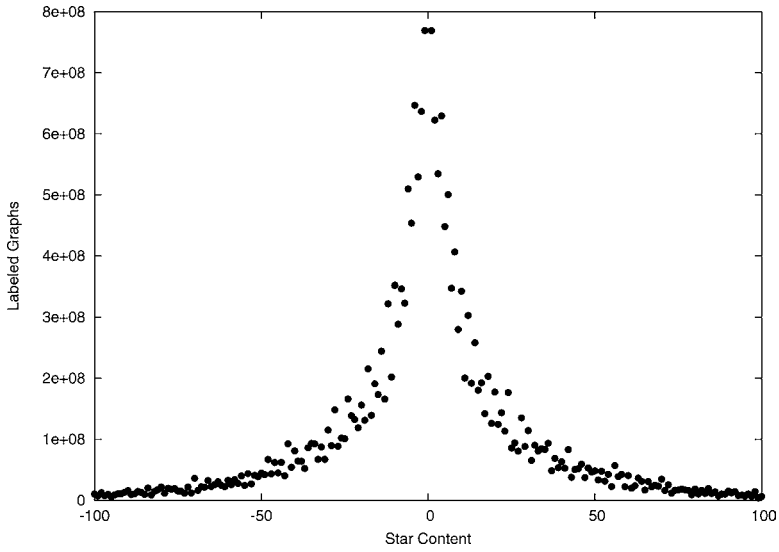**Fig. 4.** Histogram plot of number of labeled graphs versus star content for B_8.

Fig. 5. Histogram plot of number of labeled graphs versus star content for B_9.
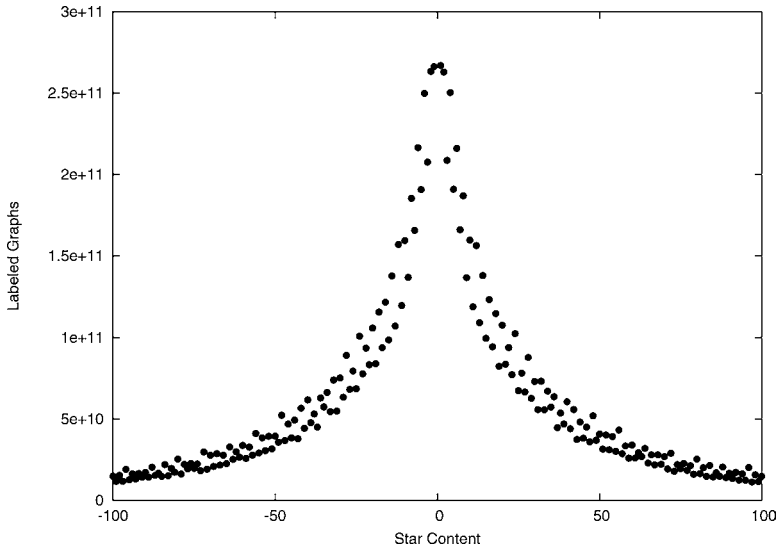

Fig. 6. Histogram plot of number of labeled graphs versus star content for B_{10}.

C SPANNING TREES USED IN THE MONTE CARLO ALGORITHM
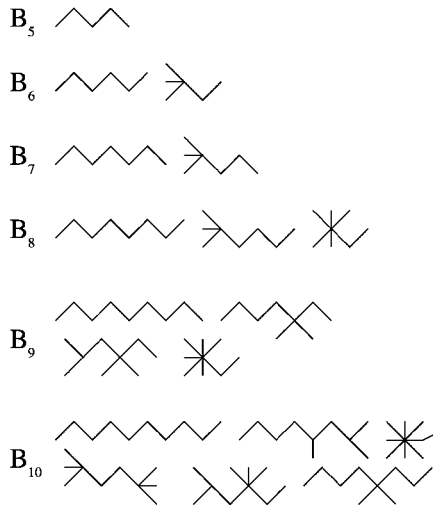

Fig. 7. Minimal sets of spanning trees for B_k, $k = 5, \cdots, 10$.

D RATIO PLOTS

Fig. 8. Ratio plot for virial coefficients in dimensions $D = 2, 3$.
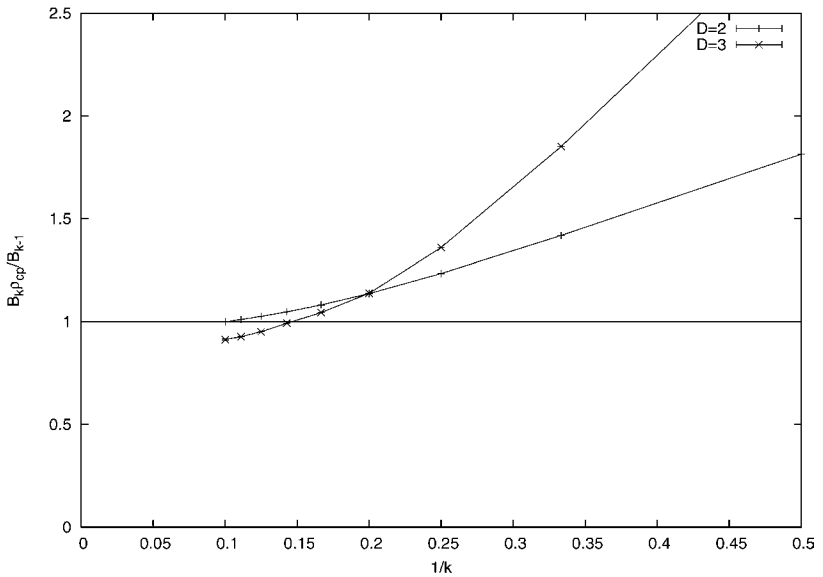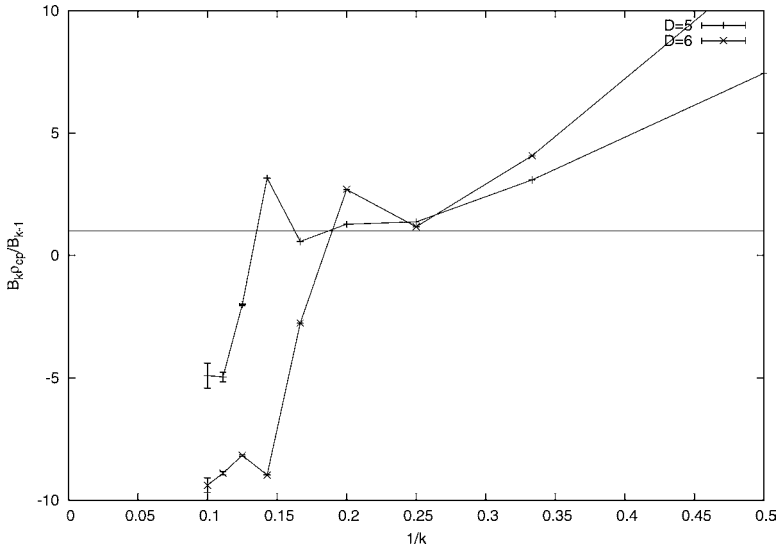
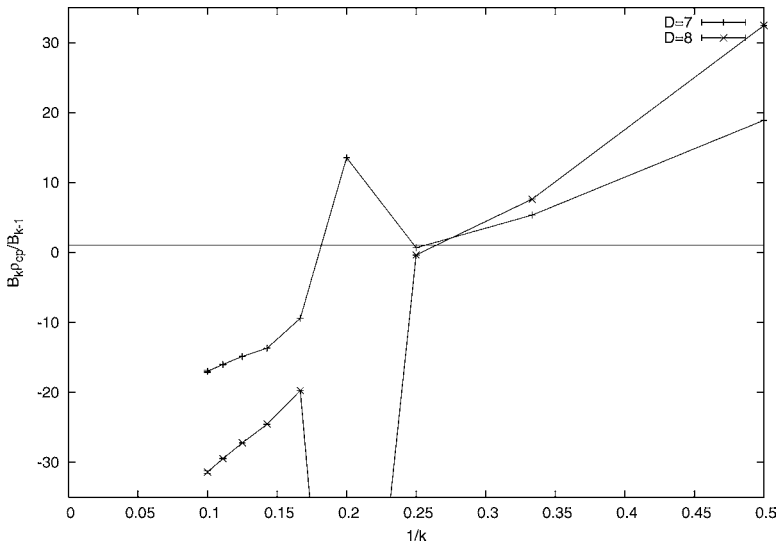**Fig. 9.** Ratio plot for virial coefficients in dimensions $D = 5, 6$.

Fig. 10. Ratio plot for virial coefficients in dimensions $D = 7, 8$.
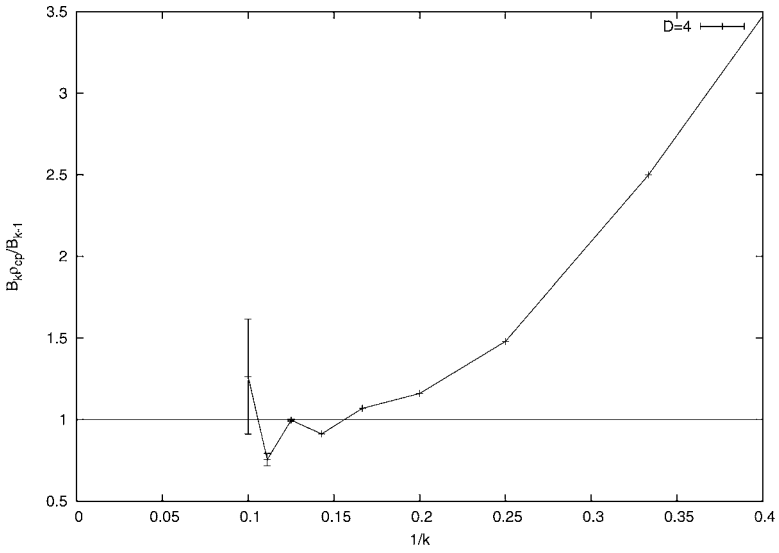
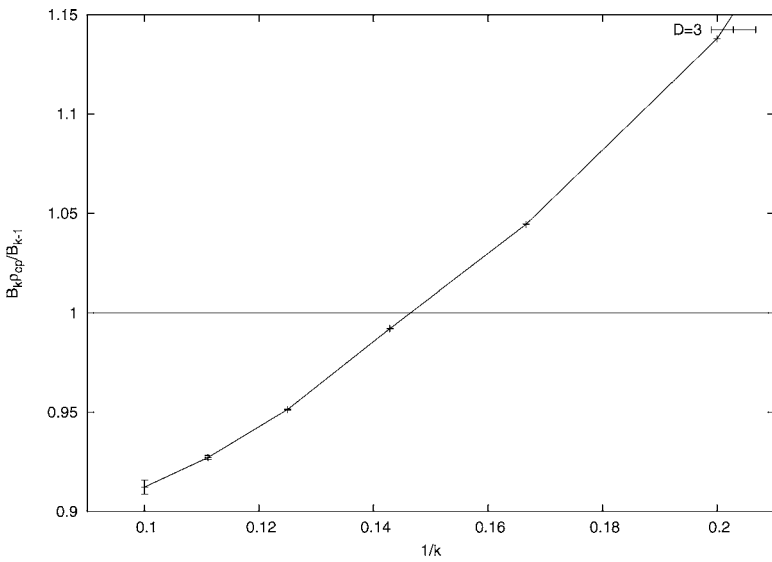**Fig. 11.** Ratio plot for virial coefficients in dimension $D = 4$.

Fig. 12. Ratio plot for virial coefficients in dimension $D = 3$ over a small domain to show non-monotonic behavior of the second derivative.

E DIFFERENTIAL APPROXIMANTS

Table VI. Singularities for all differential approximants in $D = 2$ in terms of $B_2\rho$, with the corresponding exponents immediately below. Defective approximants are marked with †, and the singularities are arranged so that the singularity nearest $B_2\rho = 1.98$ is in the left most column. In most cases, this singularity has the smallest modulus, but when this is not the case the singularity with smallest modulus is marked with ∗

Approximant	Singularity/Exponent			
[4, 3; 0]	1.98	$1.58 \pm 2.94\ i$		
	-1.74	$0.528 \mp 0.449\ i$		
[3, 4; 0]	1.98	$1.58 \pm 2.92\ i$	-30.6	
	-1.74	$0.508 \mp 0.453\ i$	0.728	
[4, 4; 0]†	1.99	$1.46 \pm 2.80\ i$	-1.11^*	
	-1.79	$0.406 \mp 0.386\ i$	3.18×10^{-5}	
[5, 4; 0]†	1.99	$1.46 \pm 2.81\ i$	-0.978^*	
	-1.79	$0.418 \mp 0.390\ i$	1.38×10^{-5}	
[4, 5; 0]†	1.99	$1.46 \pm 2.81\ i$	$-267.$	-0.977^*
	-1.79	$0.418 \mp 0.390\ i$	0.952	1.37×10^{-5}
[3, 2; 1]	1.96	-5.22		
	-1.66	12.3		
[2, 3; 1]	1.96	$-3.66 \pm 7.70\ i$		
	-1.67	$1.92 \mp 7.72\ i$		
[3, 3; 1]	$1.80 \pm 0.198\ i$	3.77		
	$-1.07 \mp 0.0804\ i$	-2.70		
[4, 3; 1]	1.98	-2.58	-0.601^*	
	-1.74	-6.19	27.3	
[3, 4; 1]	1.98	$-0.589 \pm 4.37\ i$	-0.828^*	
	-1.76	$0.0841 \mp 2.37\ i$	8.79	
[2, 2; 2]	1.96	-5.78		
	-1.66	14.0		
[3, 2; 2]	1.95	0.619^*		
	-1.59	-0.935		
[2, 3; 2]	2.06	$2.09 \pm 0.978\ i$		
	-2.25	$-0.830 \pm 1.11\ i$		
[3, 3; 2]	1.97	$0.945 \pm 1.80\ i$		
	-1.70	$-0.344 \pm 2.38\ i$		
[2, 2; 3]	1.98	0.345^*		
	-1.79	-23.7		
[3, 2; 3]	1.98	0.361^*		
	-1.78	-21.2		
[2, 3; 3]	1.98	42.6	0.445^*	
	-1.78	-3.23	-16.6	
[2, 2; 4]	1.98	-0.0937^*		
	-1.75	95.9		
[2, 2, 2; 0]	1.79	1.21		
	1.24	-10.7		
[3, 2, 2; 0]	$2.16 \pm 0.319\ i$			
	$-2.74 \mp 0.955\ i$			
[2, 3, 3; 0]	1.94	$0.939 \pm 1.61\ i^*$		
	-1.41	$-0.985 \pm 1.12\ i$		
[2, 2, 2; 1]	1.98	9.17		
	-1.72	-17.5		

Table VII. Singularities for all differential approximants in $D = 3$ in terms of $B_2\rho$, with the corresponding exponents immediately below. Defective approximants are marked with †, and the singularities are listed from left to right in order of their modulus. The most stable singularity is on the positive real axis in the vicinity of $B_2\rho = 3.75$, and this appears in the second column in all cases.

Approximant	Singularity/Exponent		
[4, 3; 0]	$-1.03 \pm 2.64\ i$	3.71	
	$0.640 \mp 0.0898\ i$	-2.04	
[3, 4; 0]	$-1.05 \pm 2.73\ i$	3.83	-6.75
	$0.752 \mp 0.134\ i$	-2.33	0.824
[4, 4; 0]	$-1.04 \pm 2.65\ i$	3.73	-65.6
	$0.652 \mp 0.0885\ i$	-2.09	14.1
[5, 4; 0]	$-1.04 \pm 2.65\ i$	3.73	$-232.$
	$0.651 \mp 0.0881\ i$	-2.09	183.
[4, 5; 0]	$-1.04 \pm 2.65\ i$	3.73	$-44.4 \pm 58.5\ i$
	$0.651 \mp 0.0881\ i$	-2.09	$0.394 \mp 9.61\ i$
[3, 2; 1]	-3.49	4.04	
	6.71	-2.95	
[2, 3; 1]	$-1.68 \pm 1.51\ i$	3.79	
	$1.72 \mp 0.928\ i$	-2.25	
[3, 3; 1]	$-1.93 \pm 1.76\ i$	3.81	
	$1.54 \mp 1.36\ i$	-2.30	
[4, 3; 1]	$-1.11 \pm 2.69\ i$	3.73	
	$0.627 \mp 0.190\ i$	-2.07	
[3, 4; 1]	$-0.621 \pm 1.87\ i$	3.79	-6.95
	$0.913 \pm 1.18\ i$	-2.24	-0.506
[2, 2; 2]	1.15	3.64	
	-3.22	-1.99	
[3, 2; 2]	-0.544	3.87	
	13.4	-2.47	
[2, 3; 2]	$-1.24 \pm 2.13\ i$	3.80	
	$1.13 \pm 0.230\ i$	-2.27	
[3, 3; 2]	$-0.464 \pm 2.25\ i$	3.78	
	$0.476 \pm 1.21\ i$	-2.22	
[2, 2; 3]	2.91	3.75	
	-1.17	-1.96	
[3, 2; 3]	2.74	3.77	
	-1.44	-2.01	
[2, 3; 3]	2.37	3.77	-38.7
	-2.05	-2.09	-3.71
[2, 2; 4]	2.78	3.77	
	-1.38	-2.00	
[2, 2, 2; 0]	4.35	-5.19	
	-3.86	4.07	
[3, 2, 2; 0]	1.21	6.04	
	-1.35	-9.45	
[2, 3, 3; 0]	$-0.840 \pm 2.45\ i$	3.76	
	$0.469 \pm 0.0986\ i$	-2.17	
[2, 2, 2; 1]	-2.68	3.70	
	6.49	-2.06	

F PADÉ APPROXIMANTS

Table VII. Singularities for all Padé approximants in $D = 2$ in terms of $B_2\rho$, with the corresponding residues immediately below. Defective approximants are marked with †.

Approximant	Singularity/Residue			
[4/3]	1.87	2.40	19.9	
	-11.5	13.7	-63.2	
[3/4]	1.91	2.21	$2.78 \pm 2.62\ i$	
	-16.8	17.4	$-0.568 \pm 0.424\ i$	
[4/4]	$1.89 \pm 0.187\ i$	$2.81 \pm 1.43\ i$		
	$-1.33 \mp 6.26\ i$	$0.839 \pm 1.90\ i$		
[5/4]	1.90	2.28	$0.513 \pm 3.21\ i$	
	-14.4	15.8	$0.0116 \mp 0.0580\ i$	
[4/5]†	-0.908	1.94	2.12	$2.60 \pm 2.40\ i$
	-4.83×10^{-7}	-26.8	27.0	$-0.380 \pm 0.551\ i$

Table VII. Singularities for all Padé approximants in $D = 3$ in terms of $B_2\rho$, with the corresponding residues immediately below. Defective approximants are marked with †.

Approximant	Singularity/Residue			
[4/3]†	0.516	3.44	3.92	
	2.84×10^{-7}	$-146.$	178.	
[3/4]	$3.32 \pm 0.602\ i$	$0.249 \pm 7.66\ i$		
	$7.42 \mp 36.9\ i$	$-1.87 \mp 5.40\ i$		
[4/4]	-2.65	$3.50 \pm 0.461\ i$	-16.3	
	0.0100	$11.9 \mp 65.0\ i$	-37.2	
[5/4]	$-1.13 \pm 2.24\ i$	$3.57 \pm 0.366\ i$		
	$0.00100 \mp 0.00669\ i$	$14.0 \mp 92.3\ i$		
[4/5]	3.43	$-1.80 \pm 3.99\ i$	4.39	6.32
	$-109.$	$0.135 \mp 0.293\ i$	213.	$-110.$

REFERENCES

1. J. D. van der Waals, *Proc. Kon. Acad. V. Wetensch, Amsterdam*, **1**:138 (1899).
2. L. Boltzmann, *Proc. Sect. Sci. K. Akad. Wet. (Amsterdam)*, (1899).
3. J. J. van Laar, *Proc. Kon. Acad. V. Wetensch, Amsterdam*, **1**:273 (1899).
4. B. J. Alder and T. E. Wainwright, Phase transition for a hard sphere system. *J. Chem. Phys.* **27**:1208–1209 (1957).

5. W. W. Wood and J. D. Jacobson, Preliminary Results from a Recalculation of the Monte Carlo Equation of State of Hard Spheres. *J. Chem. Phys.* **27**:1207–1208 (1957).

6. J. S. Rowlinson, The virial expansion in two dimensions, *Mol. Phys.* **7**:593–594 (1964).

7. P. C. Hemmer, Virial Coefficients for the Hard-Core Gas in Two Dimensions. *J. Chem. Phys.* **42**:1116–1118 (1964).

8. N. Clisby and B. M. McCoy, Analytical calculation of B_4 for hard spheres in even dimensions. *J. Stat. Phys.* **114**:1343–1361 (2004).

9. I. Lyberg, The Fourth Virial Coefficient of a Fluid of Hard Spheres in Odd Dimensions. *J. Stat. Phys.* **119**:747–764 (2005).

10. N. Metropolis, A. W. Rosenbluth, M. N. Rosenbluth and A. H. Teller, Equation of State Calculations by Fast Computing Machines. *J. Chem. Phys.* **21**:1087–1092 (1953).

11. M. N. Rosenbluth and A. W. Rosenbluth, Further Results on Monte Carlo Equations of State. *J. Chem. Phys.* **22**:881–884 (1954).

12. F. H. Ree and W. G. Hoover, Fifth and sixth virial coefficients for hard spheres and hard discs. *J. Chem. Phys.* **40**:939–950 (1964).

13. F. H. Ree and W. G. Hoover, Reformulation of the Virial Series for Classical Fluids. *J. Chem. Phys.* **41**:1635–1645 (1964).

14. F. H. Ree and W. G. Hoover, Seventh virial coefficients for hard spheres and hard discs. *J. Chem. Phys.* **46**:4181–4196 (1967).

15. E. J. Janse van Rensburg, Virial coefficients for hard discs and hard spheres. *J. Phys. A* **26**:4805–4818 (1993).

16. A. Y. Vlasov, X. M. You and A. J. Masters, Monte–Carlo integration for virial coefficients re–visited: hard convex bodies, spheres with a square–well potential and mixtures of hard spheres. *Mol. Phys.* **100**:3313–3324 (2002).

17. J. Kolafa, S. Labík and A. Malijevský, Accurate equation of state of the hard sphere fluid in stable and metastable regions. *Phys. Chem. Chem. Phys.* **6**:2335–2340 (2004).

18. S. Labík, J. Kolafa and A. Malijevský, Virial coefficients of hard spheres and hard discs up to the ninth. *Phys. Rev. E* **71**:021105 (2005).

19. F. H. Ree and W. G. Hoover, On the signs of the hard sphere virial coefficients. *J. Chem. Phys.* **40**:2048–2049 (1964).

20. M. Bishop, A. Masters and J. H. R. Clarke, Equation of state of hard and Weeks–Chandler–Anderson hyperspheres in four and five dimensions. *J. Chem. Phys.* **110**:11449–11453 (1999).

21. M. Bishop, A. Masters and A. Y. Vlasov, Higher virial coefficients of four and five dimensional hard hyperspheres. *J. Chem. Phys.* **121**:6884–6886 (2004).

22. M. Bishop, A. Masters and A. Y. Vlasov, The Eighth Virial Coefficient of Four and Five Dimensional Hard Hyperspheres. *J. Chem. Phys.* **122**:154502 (2005).

23. M. Bishop, P. A. Whitlock and D. Klein, The Structure of Hyperspherical Fluids in Various Dimensions. *J. Chem. Phys.* **122**:074508 (2005).

24. M. Bishop and P. A. Whitlock. The Equation of State of Hard Hyperspheres in Four and Five Dimensions. *J. Chem. Phys.* **123**: 014507 (2005).

25. H. L. Frisch, N. River and D. Wyler, Classical Hard-Sphere Fluid in Infinitely Many Dimensions. *Phys. Rev. Lett.* **54**:2061–2063 (1985).

26. H. L. Frisch and J. K. Percus, High dimensionality as an organizing device for classical fluids. *Phys. Rev. E* **60**:2942–2948 (1999).

27. N. Clisby and B. M. McCoy, Negative virial coefficients and the dominance of loose packed diagrams for D–dimensional hard spheres. *J. Stat. Phys.* **114**:1361–1392 (2004).

28. N. Clisby, *Negative Virial Coefficients for Hard Spheres*. PhD thesis, Stony Brook University, Stony Brook, New York, May (2004).

29. K. W. Kratky, A New Graph Expansion of Virial Coefficients. *J. Stat. Phys.* **27**:533–551 (1982).

30. J. E. Mayer and M. G. Mayer, *Statistical Mechanics*. Wiley (1940).

31. J. K. Percus and G. J. Yevick, Analysis of Classical Statistical Mechanics by Means of Collective Coordinates. *Phys. Rev.* **110**:1–13 (1958).

32. J. K. Percus (eds.) The Pair Distribution Function in Classical Statistical Mechanics, in H. L. Frisch and J. L. Lebowitz, *The Equilibrium Theory of Classical Fluids*, pp. II–33–II–170. (W. A. Benjamin, Inc., New York 1964).

33. B. D. McKay, Practical Graph Isomorphism. *Congressus Numerantium*, **30**:45–87 (1981).

34. H. N. Gabow and E. W. Myers, Finding All Spanning Trees of Directed and Undirected Graphs. *SIAM J. Comput.* **7**:280–287 (1978).

35. R. M. Ziff, Four-tap shift-register-sequence random-number generator. *Comp. in Phys.* **12**:385–392 (1998).

36. D. E. Knuth, *The Art of Computer Programming: Fundamental Algorithms*, Addison-Wesley, third edition (1997) Vol 1.

37. S. Banerjia and R. A. Dwyer, Generating Random Points in a Ball. *Commun. Stat. Sim.* **22**:1205–1209 (1993).

38. D. J. Rose, R. E. Tarjan and G. S. Lueker, Algorithmic Aspects of Vertex Elimination on Graphs. *SIAM J. Comput.* **5**:266–283 (1976).

39. R. E. Tarjan and M. Yannakakis, Simple Linear-Time Algorithms to Test Chordality of Graphs, Test Acyclicity of Hypergraphs, and Selectively Reduce Acyclic Hypergraphs. *SIAM J. Comput.* **13**:566–579 (1984).

40. R. E. Tarjan, Decomposition by Clique Separators. *Disc. Math.* **55**:221–232 (1985).

41. S. H. Whitesides, An Algorithm for Finding Clique Cut-Sets. *Inf. Proc. Lett.* **12**:31–32 (1981).

42. B. J. Alder and T. E. Wainright, Phase Transition in Elastic Disks. *Phys. Rev.* **127**:359–361 (1962).

43. W. W. Wood, Monte Carlo studies of simple liquid models, in *Physics of Simple Liquids*, (North Holland, Amsterdam 1968) pp. 115–230.

44. J. P. J. Michels and N. J. Trappeniers, Dynamical computer simulations on hard hyperspheres in four- and five-dimensional space. *Phys. Lett.* **104**:425–429 (1984).

45. A. Jaster, Computer simulations of the two-dimensional melting transition using hard disks. *Phys. Rev. E* **59**:2594–2602 (1999).

46. J. G. Dash, History of the search for continuous melting. *Rev. Mod. Phys.* **71**:1737–1743 (1999).

47. K. Binder, S. Sengupta and P. Nielaba, The liquid–solid transition of hard discs: first-order transition or Kosterlitz–Thouless–Halperin–Nelson–Young scenario? *J. Phys.: Condens. Matter* **14**:2323–2333 (2002).

48. A. Jaster, The hexatic phase of the two-dimensional hard disk system. *Phys. Lett. A* **330**:120–125 (2004).

49. B. J. Alder and T. E. Wainright, Studies in molecular dynamics 2: behavior of small numbers of elastic hard spheres. *J. Chem. Phys.* **33**:1439 (1960).

50. W. G. Hoover and F. H. Ree, Melting transition and communal entropy for hard spheres. *J. Chem. Phys.* **49**:3609–3617 (1968).

51. G. Nebe and N. J. A. Sloane, A Catalogue of Lattices, http://www.research.att.com/~njas/lattices/index.html.

52. J. L. Lebowitz and O. Penrose, Convergence of virial expansion. *J. Math. Phys.* **5**:841 (1964).

53. M. E. Fisher, The Nature of Critical Points, in *Lectures in Theoretical Physics VII*, (University of Colorado Press, Boulder, Colorado 1965) pp. 73–109.

54. S. N. Isakov, Nonanalytic Features of the First Order Phase Transition in the Ising Model. *Commun. Math. Phys.* **95**:427–443 (1984).

55. J. Groeneveld, Two Theorems on Classical Many-Particle Systems. *Phys. Lett.* **3**:50–51 (1962).

56. M. E. Fisher, Bounds for the Derivatives of the Free Energy and the Pressure of a Hard-Core System near Close Packing. *J. Chem. Phys.* **42**:3852–3856 (1965).

57. W. G. Hoover, Bounds on the Configurational Integral for Hard Parallel Squares and Cubes. *J. Chem. Phys.* **43**:371–374 (1965).

58. E. Thiele, Equation of State for Hard Spheres. *J. Chem. Phys.* **39**:474–479 (1963).
59. M. S. Wertheim, Exact Solution of the Percus-Yevick Integral Equation for Hard Spheres. *Phys. Rev. Lett.* **10**:321–323 (1963).
60. M. S. Wertheim, Analytic solution of the Percus–Yevick equation. *J. Math Phys.* **5**:643 (1964).
61. H. Reiss, H. L. Frisch and J. L. Lebowitz, Statistical mechanics of rigid spheres. *J. Chem. Phys.* **31**:369–380 (1959).
62. E. A. Guggenheim, Variations on van der Waals equation of state for high densities. *Mol. Phys.* **9**:199 (1965).
63. N. F. Carnahan and K. E. Starling, Equation of State for Nonattracting Rigid Spheres. *J. Chem. Phys.* **51**:635–636 (1969).
64. J. I. Goldman and J. A. White, Equation of state for the hard-sphere gas. *J. Chem. Phys.* **89**:6403–6405 (1988).
65. R. Hoste and J. D. Dael, Equation of state for hard–sphere and hard–disk systems. *J. Chem Soc. Faraday Trans. 2* **80**:477–488 (1984).
66. J. D. Bernal and J. Mason, Co–ordination of randomly packed spheres. *Nature* **188**:910–911 (1960).
67. J. D. Bernal, Bakerian Lecture 1962 – The structure of liquids. *Proc. Roy. Soc. Lond. A* **280**:299–322 (1964).
68. G. D. Scott, Packing of equal spheres. *Nature* **188**:908–909 (1960).
69. J. L. Finney, Random packings and the structure of simple liquids I. The geometry of random close packing. *Proc. Roy. Soc. Lond. A* **319**:479–493 (1970).
70. E. J. Le Fevre, Equation of State for Hard-sphere Fluid. *Nature Phys.* **235**:20 (1972).
71. D. Ma and G. Ahmadi, An equation of state for dense rigid sphere gases. *J. Chem. Phys.* **84**:3449 (1986).
72. Y. Song, R. M. Stratt and A. E. Mason, The equation of state of hard spheres and the approach to random closest packing. *J. Chem. Phys.* **88**:1126–1133 (1988).
73. S. Jasty, M. Al-Naghy and M. de Llano, Critical exponent for glassy packing of rigid spheres and disks. *Phys. Rev. A* **35**:1376–1381 (1987).
74. S. Torquato, Mean Nearest–Neighbor Distance in Random Packings of Hard D–Dimensional Spheres. *Phys. Rev. Lett.* **74**:2156–2159 (1995).
75. S. Torquato, Nearest–neighbor statistics for packings of hard spheres and disks. *Phys. Rev. E* **51**:3170–3182 (1995).
76. B. C. Freasier and D. J. Isbister, A remark on the Percus–Yevick approximation in higher dimensions. *Mol. Phys.* **42**:927–936 (1981).
77. E. Leutheusser, Exact Solution of the Percus–Yevick Equation for a Hard–Core Fluid in Odd Dimensions. *Physica A* **127**:667–676 (1984).
78. M. Robles, M. López de Haro and A. Santos, Equation of state of a seven-dimensional hard-sphere fluid. Percus–Yevick theory and molecular-dynamics simulations. *J. Chem. Phys.* **120**:9113–9122 (2004).
79. A. Baram and M. Luban, Divergence of the virial series for hard discs and hard spheres at closest packing. *J. Phys. C: Solid St. Phys.* **12**:L659–L664 (1979).
80. I. C. Sanchez, Virial coefficients and close–packing of hard spheres and disks. *J. Chem. Phys.* **101**:7003–7006 (1994).
81. D. S. Gaunt and G. S. Joyce, Virial expansions for hard-core fluids. *J. Phys. A* **13**:L211–L216 (1980).
82. A. J. Guttmann, Asymptotic Analysis of Power-Series Expansions, in C. Domb and J. Lebowitz, editors, *Phase Transitions and Critical Phenomena*, volume 13, chapter 1, (Academic Press, 1989) pp. 1–234.
83. R. J. Baxter Hard hexagons – exact solution. *J. Phys. A* **13**:L61–70 (1980).
84. M. P. Richey and C. A. Tracy, Equation of state and isothermal compressibility for the hard hexagon model in the disordered regime. *J. Phys. A* **20**:L1121–L1126 (1987).

85. G. S. Joyce, On the Hard-Hexagon Model and the Theory of Modular Functions. *Phil. Trans. R. Soc. Lond. A* **325**:643–702 (1988).
86. R. J. Baxter, Three-Colorings of the Square Lattice: A Hard Squares Model. *J. Math. Phys.* **11**:3116–3124 (1970).
87. W. G. Hoover and A. G. de Rocco, Sixth and Seventh Virial Coefficients for the Parallel Hard-Cube Model. *J. Chem. Phys.* **36**:3141–3161 (1962).
88. G. E. Uhlenbeck and G. W. Ford, The Theory of Linear Graphs with Applications to the Theory of the Virial Development of the Properties of Gases. In *Studies in Statistical Mechanics*, (North Holland 1962) Vol 1, pp. 119–211.
89. A. Baram and J. S. Rowlinson, Studies of the Gaussian model 1. The one-component system. *Mol. Phys.* **74**:707–713 (1991).
90. A. J. Guttmann and G. S. Joyce, On a new method of series analysis in lattice statistics. *J. Phys. A* **5**:L81–L84 (1972).
91. G. S. Joyce and A. J. Guttmann, A New Method of Series Analysis, In P. R. Graves-Morris, editor, *Padé Approximants and Their Applications*, (Academic Press 1973) pp. 163–167.
92. D. L. Hunter and G. A. Baker, Methods of Series Analysis. I. Comparison of Current Methods Used in the Theory of Critical Phenomena. *Phys. Rev. B* **7**:3346–3376 (1973).
93. D. L. Hunter and G. A. Baker, Methods of series analysis. III. Integral approximant methods. *Phys. Rev. B* **19**:3808–3821 (1979).
94. M. E. Fisher and H. Au-Yang, Inhomogeneous differential approximants for power series. **12**:1677–1692 (1979).
95. N. Clisby, Ninth and Tenth Order Virial Coefficients for Hard Spheres in *D* Dimensions – Collection of Tables, http://www.ms.unimelb.edu.au/~nclisby/papers/papers.html.